ARTICLES
https://doi.org/10.1038/s41551-018-0219-9
nature biomedical engineering

Effects of 3D culturing conditions on the transcriptomic profile of stem-cell-derived neurons

Halil Tekin[1,2*], Sean Simmons[1], Beryl Cummings[1,3], Linyi Gao[1,4], Xian Adiconis[1], Cynthia C. Hession[1], Ayan Ghoshal[1], Danielle Dionne[1], Sourav R. Choudhury[1,2], Volkan Yesilyurt[5], Neville E. Sanjana[1,2,7], Xi Shi[1], Congyi Lu[1,2,7], Matthias Heidenreich[1,2], Jen Q. Pan[1], Joshua Z. Levin[1] and Feng Zhang[1,2,4,6]

Understanding neurological diseases requires tractable genetic systems, and engineered three-dimensional (3D) neural tissues are an attractive choice. Yet how the cellular transcriptomic profiles in these tissues are affected by the encapsulating materials and are related to the human brain transcriptome is not well understood. Here, we report the characterization of the effects of different culturing conditions on the transcriptomic profiles of induced neuronal cells and developed a method for the rapid generation of 3D co-cultures of neuronal and astrocytic cells from the same pool of human embryonic stem cells. By comparing the gene-expression profiles of neuronal cells in culture conditions relevant to the developing human brain, we found that modifying the degree of crosslinking of composite hydrogels can tune expression patterns so that they correlate with those of specific brain regions and developmental stages. Moreover, single-cell-sequencing results showed that our engineered tissues recapitulate transcriptional patterns of cell types in the human brain. Analyses of culturing conditions will inform the development of 3D neural tissues for use as tractable models of brain diseases.

There is increasing evidence to indicate that some neurological diseases have a genetic component[1–3] as evidenced by the growing catalogues of gene variants involved in these diseases generated by next-generation sequencing[2,4,5]. Understanding the mechanistic outcomes of these mutations, however, has been difficult because we lack tractable genetic models in which to systematically interrogate them. One promising approach has been to engineer 3D neural tissues[6–9] that can provide a system for rapid genetic manipulation in a brain-like environment. To be effective, such tissues should closely reflect the extracellular matrix (ECM), gene expression profiles and cell composition of the human brain. In addition, they should be rapid and simple to generate and produce controllable numbers of brain-related cell types with an isogenic background within a tunable environment.

A number of approaches have been taken to develop such neural tissues in vitro. These approaches focus on differentiating human embryonic stem cells (hESCs) and induced pluripotent stem cells (iPSCs) into brain-related cell types, such as neurons and glia, on two-dimensional (2D) surfaces as well as 3D matrices[10–16]. Typically, the brain-like properties of these tissues are assessed by performing electrophysiological assays and immunostainings for neural markers. However, these broad approaches may not accurately reflect the cellular state, and more comprehensive analyses, such as RNA sequencing (RNA-seq), could improve assessments of these tissues. A previous study compared the transcriptomic profile of cerebral organoids to that of the human fetal brain[17]; however, it has not been reported how the global transcriptome of neural cells in engineered tissues relates to the human brain and how the gene expression profiles of these cells respond to various culturing conditions.

To generate a system that can serve as a proxy for studying the genetics of the human brain, we compared a number of different conditions used for generating 3D neural tissues from induced neuronal (iN) cells from hESCs. We also developed a method for rapidly generating 3D co-cultures of iN and astrocytic cells derived from the same population of hESCs. iN cells can be efficiently produced directly from hESCs through the ectopic expression of transcription factors[18–22] and have been used to model neurological diseases by culturing them on 2D surfaces[23,24]. This approach has also been used to produce 3D neural tissues on an electrospun scaffold, which are then used for transplantation[25]. We extended these approaches to create a 3D culture of iN cells within Matrigel, a basement membrane matrix that includes components that closely reflect the ECM in the brain[6,26]. The effects of the addition of hyaluronic acid (HA) and the formation of composite hydrogels (CHs) of Matrigel and alginate with varying crosslinking density and volume for optimizing the components of these tissues were also explored. We compared the transcriptome of these iN cells to a panel of human brain transcriptomic data and showed that the gene expression of iN cells can be tuned to correlate with specific developmental time points and brain regions by modulating the composition of the 3D matrix. Single-cell sequencing of cells co-cultured in 3D tissues confirmed their transcriptomic correlations to cell types found in the human brain. Finally, we used gene editing tools to knockout genes in our 3D tissues that are implicated in neurodegenerative diseases to demonstrate the feasibility of combining these technologies.

Results

Development and optimization of 3D neural tissues from hESCs. To create a robust, genetically tractable 3D neural tissue system, we

[1]Broad Institute of MIT and Harvard, Cambridge, MA, USA. [2]McGovern Institute for Brain Research, Massachusetts Institute of Technology, Cambridge, MA, USA. [3]Analytical and Translational Genetics Unit, Massachusetts General Hospital, Boston, MA, USA. [4]Department of Biological Engineering, Massachusetts Institute of Technology, Cambridge, MA, USA. [5]Koch Institute for Integrative Cancer Research, Massachusetts Institute of Technology, Cambridge, MA, USA. [6]Department of Brain and Cognitive Sciences, Massachusetts Institute of Technology, Cambridge, MA, USA. [7]Present address: New York Genome Center and Department of Biology, New York University, New York, NY, USA. *e-mail: halil@alum.mit.edu

used a transcriptional activation approach to differentiate iN cells from hESCs, which were then encapsulated in a Matrigel matrix (Fig. 1a). First, we tested whether hESCs transduced with constructs that overexpress *NGN1* and *NGN2* and encapsulated in a Matrigel 3D matrix could directly differentiate into iN cells . However, this approach resulted in aggregation of encapsulated cells within 5 days (Supplementary Fig. 1a), preventing efficient differentiation. To circumvent aggregation, hESCs were first seeded on 2D plates and then induced to form neuronal cells, which were subsequently detached and then encapsulated in Matrigel (Supplementary Fig. 1b). This process led to less aggregation; however, aggregates continued to form over time, with spheroids present at day 30 (Supplementary Fig. 1c,d). Further improvements were made by increasing the selection for constructs expressing *NGN1* and *NGN2* and introducing a proliferation inhibitor, 1-β-D-arabinofuranosylcytosine (Ara-C), to suppress the proliferation of undifferentiated stem cells. This approach resulted in 3D, pure human neural tissues without cell aggregates (Supplementary Fig. 1e, Supplementary Videos 1–3). For comparison, we also generated 2D cultures of iN cells (Fig. 1a, and Methods).

Characterization of 3D cultures. Characterization of the differences between 2D and 3D cultures of iN cells using global transcriptome analysis demonstrated clear differences between these cultures at both the week 1 and week 5 time points (Fig. 1c, Supplementary Tables 1, 2). As maintaining healthy neural tissues for an extended amount of time promotes neuronal maturity[13,22], we focused our analysis on tissues at the week 5 time point. Gene set enrichment analysis (GSEA) showed more enriched neurological processes present in 3D cultured iN cells than in 2D ones at 5 weeks, whereas 2D cultures were enriched for apoptosis and oxidative stress markers, indicative of their poor health (Supplementary Fig. 2a). We validated a subset of these genes by quantitative PCR (qPCR) (Supplementary Fig. 2b). This validation was supported by a gene ontology (GO) analysis for upregulated and downregulated genes with $P<0.001$ (Fig. 1f). This trend was not significantly affected by batch-to-batch variation in Matrigel (Supplementary Fig. 3a–c). Given this trend, we next tested whether increasing the concentration of Matrigel would further enhance the enrichment of neurological processes, and we found an incremental improvement (Supplementary Fig. 3d,e). The ability to study the electrophysiological properties of tissues in a 3D culture system is desirable for downstream genetic studies. Therefore, we analysed the expression of genes involved in channel activity and the electrophysiological properties of these tissues. The 3D cultures of iN cells showed an increased expression of a number of genes involved in channel activity, and we found that these cells, unlike their 2D counterparts, were capable of firing repetitive action potentials and displayed spontaneous excitatory postsynaptic currents (Supplementary Fig. 4). To further develop the cellular composition of our 3D cultures, we co-cultured iN cells with mouse astrocytes, which support neuronal processes and functions[18,19,27] (Fig. 1b) and performed bulk RNA-seq (reads from mouse astrocytes were filtered out, see Supplementary Fig. 5a and Methods). We observed global transcriptome differences between 2D and 3D co-cultures of iN cells at both the week 1 and week 5 time points (Fig. 1d, Supplementary Table 3), and a substantial number of the significantly upregulated genes in 3D co-culture conditions were also upregulated in iN cells cultured in 3D without mouse astrocytes (Fig. 1e). Although cells in both 3D and 2D co-cultures at longer time points were electrophysiologically active (Supplementary Fig. 6), a GO analysis of significantly upregulated and downregulated genes ($P<0.001$) at week 5 revealed more enriched neurological processes in 3D co-cultured iN cells versus the 2D counterparts (Fig. 1g). The 3D co-cultured tissues showed clear transcriptional differences to that of pure iN cell 3D cultures and upregulation of genes involved in neurological processes (Supplementary Fig. 5b,c). We therefore used 3D co-cultured tissues for further analyses.

Influence of HA on the transcriptome of 3D co-cultured iN cells. Previous neural tissue engineering approaches have incorporated HA, a non-sulfated glycosaminoglycan, into the matrix to mimic biological conditions[26,28–31]; however, the influence of HA on the transcriptome of tissues has not yet been characterized by genome-wide profiling. We incorporated high molecular mass (~$1.5–1.8\times10^6$ Da) HA at two different concentrations in our tissue system (Fig. 2a) and then performed bulk RNA-seq at 5 weeks. The presence of HA resulted in significant differences in the transcriptome of iN cells (Fig. 2b). GSEA and GO analysis showed that cells cultured in the absence of HA were enriched for neurological processes, whereas cells cultured in the presence of HA were enriched in non-neuronal biological processes (Fig. 2c, Supplementary Fig. 7a, Supplementary Table 4). Previous studies have reported increased transcription of some neuronal genes in the presence of HA[29]; therefore, we specifically looked at the expression of genes involved in neuron development, forebrain development, central nervous system development and channel activity. Genes such as *DLG4*, *NEUROD4* and *CLU* were expressed at high levels in the presence of HA (Supplementary Fig. 7b). To gain a global view of the effect of HA on gene expression patterns, we compared the transcriptomes of our engineered tissues cultured in the presence and absence of HA to the human brain transcriptome of four different subregions at four fetal developmental stages. The following four subregions were compared: V1C: primary visual cortex (striate cortex, area V1/17); DFC: dorsolateral prefrontal cortex; A1C: primary auditory cortex (core); and M1C: primary motor cortex (area M1, area 4). The four fetal developmental stages analysed were 12 post-conceptual weeks (pcw), 16 pcw, 19 pcw and 37 pcw. We found that the presence of HA broadly decreased the correlation between the transcriptome of 3D co-cultured iN cells to the human brain developmental transcriptome, although correlations to 37 pcw did not fit this trend (Fig. 2d).

Transcriptome profiles can be tuned using CHs. The differentiation of cells in and the gene expression profiles of 3D tissues can be affected by the mechanical stiffness of the matrix[29,32–35], providing an avenue for creating tunable engineered tissues. As increasing the concentration of Matrigel had minimal effect, we explored how a CH consisting of alginate and Matrigel affected gene expression profiles (Fig. 3a). Alginate networks can be created in the Matrigel through the addition of calcium as a crosslinker, whereby the concentration of calcium can be increased to produce a stiffer matrix[33] (Supplementary Fig. 8a). We performed bulk RNA-seq on co-cultured iN cells at week 5 in Matrigel and in CHs with increasing amounts of crosslinker. Principal component analysis (PCA) showed clear transcriptomic differences in the CHs relative to Matrigel alone, although the global gene expression profiles of CHs with intermediate levels of crosslinker were not strongly separated from each other (Fig. 3b). A global differential expression analysis of the transcriptomes of iN cells in CHs versus those in the Matrigel hydrogel showed four distinct clusters of genes with different patterns of expression. These clusters contained a number of genes relevant to human neurological disease such as amyotrophic lateral sclerosis (ALS) (for example, *SOD1*) and autism spectrum disorder (ASD) (for example, *ADSL*) (Fig. 3c, Supplementary Fig. 9, Supplementary Table 5). We also looked at the differential expression of genes involved in forebrain development, axon guidance and neuron development biological processes (Fig. 3c, Supplementary Fig. 8b–d). To analyse the effect of increasing the crosslinker concentration in CHs on the gene expression profile of iN cells, we performed differential expression analysis of our RNA-seq data relative to the CH with the lowest level of crosslinker. In particular,

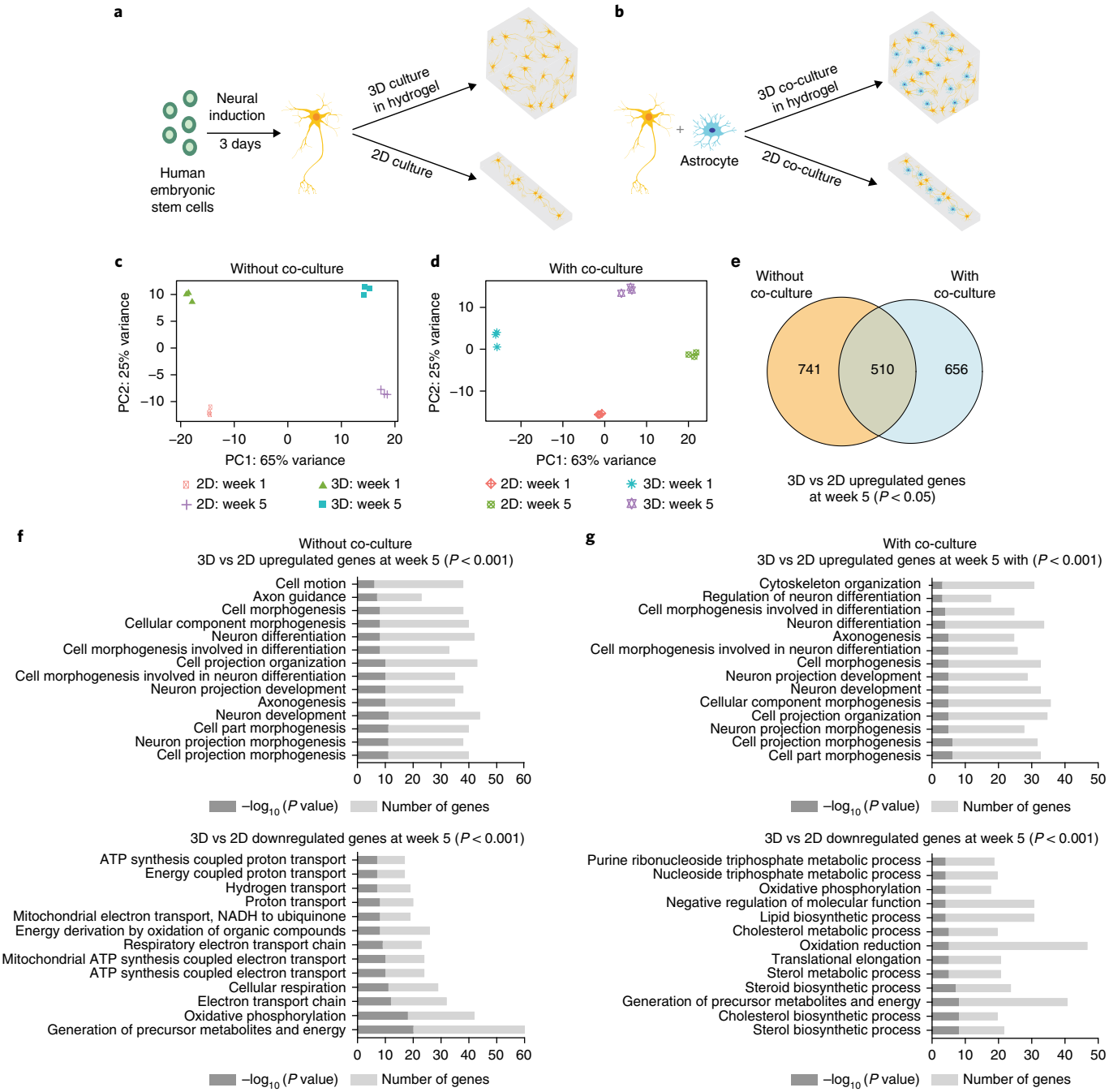

Fig. 1 | 3D cultures and co-cultures of hESC-derived human iN cells within Matrigel show enriched neuronal processes compared with 2D cultures and co-cultures. a, Schematic for generating 3D and 2D neuronal cultures of human iN cells derived directly from hESCs by transcriptional activation (see also Supplementary Fig. 1 and Methods for details). **b**, Schematic for generating 3D and 2D neuronal co-cultures of human iN cells and mouse astrocytes. **c**, PCA of gene expression values derived from whole transcriptome sequencing data of 3D and 2D cultured iN cells at weeks 1 and 5 ($n = 3$ for each condition). For 3D cultures, human iN cells (at a concentration of 10×10^6 cells ml^{-1}) were encapsulated in Matrigel (4.6 mg ml^{-1}). **d**, PCA of gene expression values derived from whole transcriptome sequencing data of 3D and 2D co-cultured iN cells at weeks 1 and 5 ($n = 3$ for each condition). For 3D co-cultures, human iN cells and mouse astrocytes (at a concentration of 20×10^6 cells ml^{-1}) were encapsulated in Matrigel (4.6 mg ml^{-1}). **e**, Venn diagram of the number of differentially upregulated genes with $P < 0.05$ for 3D versus 2D cultures and co-cultures and overlap of genes at week 5 (adjusted P value is 0.05). **f**,**g**, GO analysis of differentially upregulated and downregulated genes with $P < 0.001$ for 3D versus 2D cultures (**f**) and co-cultures (adjusted P value is 0.05) (**g**).

we focused on differentially expressed genes involved in forebrain development, axon guidance and neuron development biological processes (Fig. 4a, Supplementary Fig. 10). Neuronal transcripts such as *DLG4, NFIB* and *UNC5C* were expressed at lower levels in iN cells co-cultured in CHs with high levels of crosslinker than in iN cells co-cultured in other CHs (Fig. 4a, Supplementary Fig. 10). Although increasing the crosslinker concentration in CHs increased the expression of *ARHGEF12*, *GSK3B*, *SLC4A7* and *GPM6A*, neuronal genes such as *ID4* and *BAD* were more highly expressed in iN cells co-cultured in CHs with intermediate levels of crosslinker than

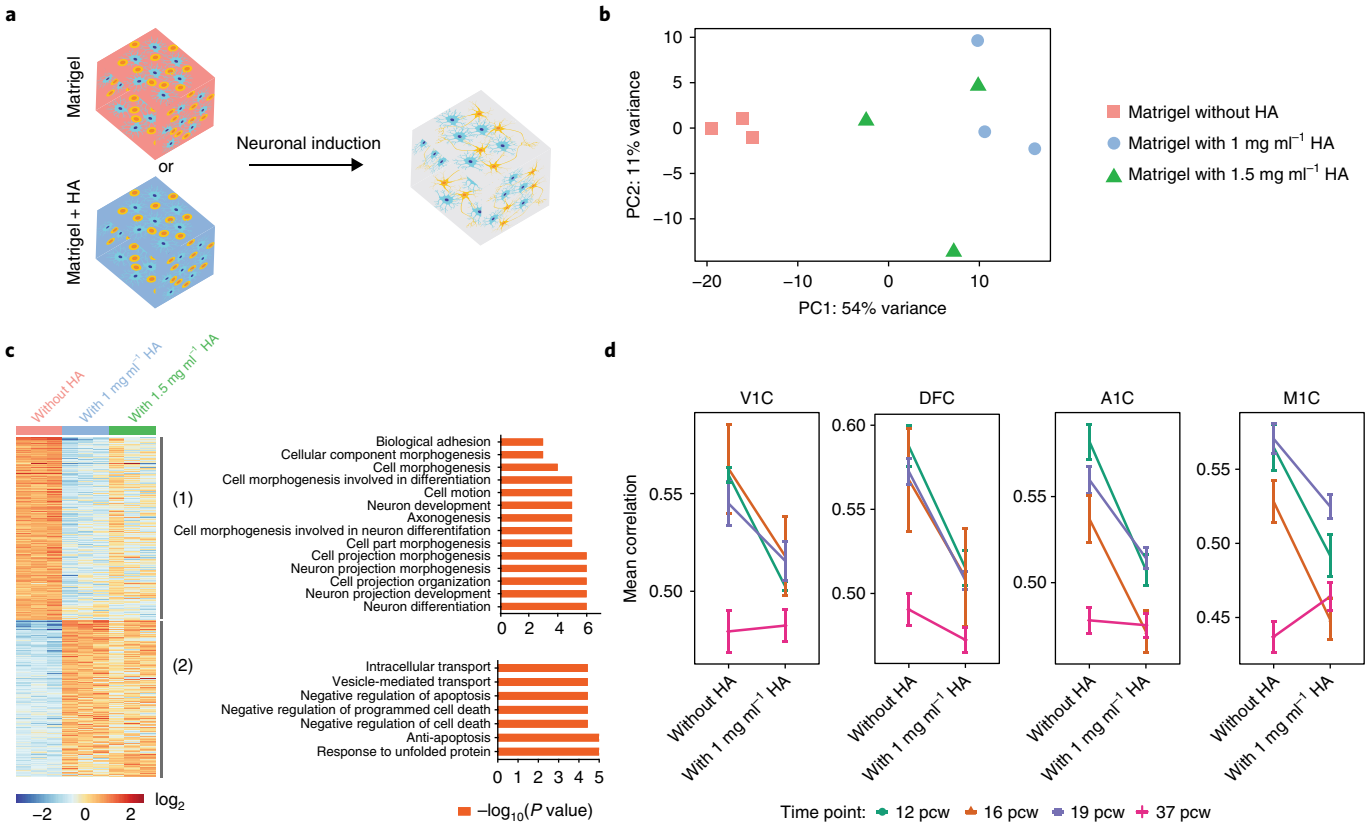

Fig. 2 | Incorporating HA within Matrigel leads to enriched non-neuronal biological processes in 3D co-cultured human iN cells and decreases the gene expression correlation to the human brain developmental transcriptome. a, Schematic showing human iN cells and mouse astrocytes (at a concentration of 30×10^6 cells ml^{-1}) encapsulated in Matrigel with or without HA trapped within the Matrigel. **b**, PCA of gene expression values derived from whole transcriptome sequencing data of 3D co-cultured iN cells in Matrigel with or without HA at week 5 of culture ($n=3$ for each condition). **c**, Gene expression clusters for iN cells co-cultured in Matrigel with or without HA. Two clusters, labelled 1 and 2, were identified (see also Supplementary Table 4). GO terms for genes in each cluster are shown. Differentially expressed genes with $P<0.01$ and $\log_2$ (fold change) <-1 or $\log_2$ (fold change) >1 were used. **d**, Pearson's correlation between RNA-seq data of iN cells with or without HA at week 5 and human brain transcriptome data of four different subregions (V1C, DFC, A1C and M1C) at four fetal developmental stages (12, 16, 19 and 37 pcw) from the BrainSpan database (http://www.brainspan.org). Bars show the mean correlation ± s.e.m.

in iN cells co-cultured in CHs with low or high levels crosslinker (Fig. 4a, Supplementary Fig. 10).

We further examined the influence of co-culturing iN cells in Matrigel hydrogel versus in CHs for 5 weeks by comparing their transcriptomes to a panel of human brain transcriptome samples. For all four subregions tested, we observed a positive trend in the correlation between the transcriptome of co-cultured iN cells to the human brain transcriptome at later developmental time points (19 pcw and 37 pcw) when moving from Matrigel to CHs with increasing levels of crosslinker (Fig. 4b). Although there were some exceptions to this trend, in most cases, culturing in CHs was an improvement over culturing in Matrigel alone. At the earliest developmental time point (12 pcw), the gene expression profile of iN cells co-cultured in Matrigel alone correlated more closely with the human data. We then determined which genes were driving the increased correlation to the human brain transcriptome at later developmental time points (19 pcw and 37 pcw) when moving from Matrigel to the CH with 4X crosslinker. To this end, we scored each gene (see Methods) and generated ranked lists for each time point (19 pcw and 37 pcw) and brain region (V1C, DFC, A1C and M1C). High scoring genes exhibited similar expression levels in the human brain developmental transcriptome and the CH with 4X crosslinker condition, but different expression levels in the human brain developmental transcriptome and the Matrigel condition (Supplementary Tables 6–13). The GO analysis for high scoring genes (rank score >3) for each brain region at 19 pcw showed enrichment for neuron-related processes, whereas high scoring genes (rank score >3) for each brain region at 37 pcw demonstrated enrichment for ECM-related processes (Supplementary Tables 6–13). Additionally, we investigated how the presence of HA and an increased cell density in the CHs affected gene expression profiles. In agreement with our previous findings, adding HA to the CH decreased the correlation between the transcriptome of co-cultured iN cells and the human brain transcriptome, whereas increasing the cell density led to similar trends (Supplementary Fig. 11). We also investigated the effect of varying the volume of the CH with or without HA on the gene expression profile of co-cultured iN cells. We found that decreasing the volume improved the enrichment of neurological processes while marginally decreasing the correlation to the human brain transcriptome (Supplementary Fig. 12).

To compare broadly all the conditions tested, we performed a differential expression analysis of all conditions relative to stem cells. In agreement with our previous results, we found that stem cells were enriched for cell cycle and cell division processes and depleted for neurogenesis and neuronal developmental processes. 2D cultures showed marginal differences, whereas 3D cultures, with the exception of the HA condition, showed the opposite pattern, whereby neuronal-related processes were enriched for and the expression of cell cycle and cell division genes was reduced (Supplementary Fig. 13, Supplementary Table 14).

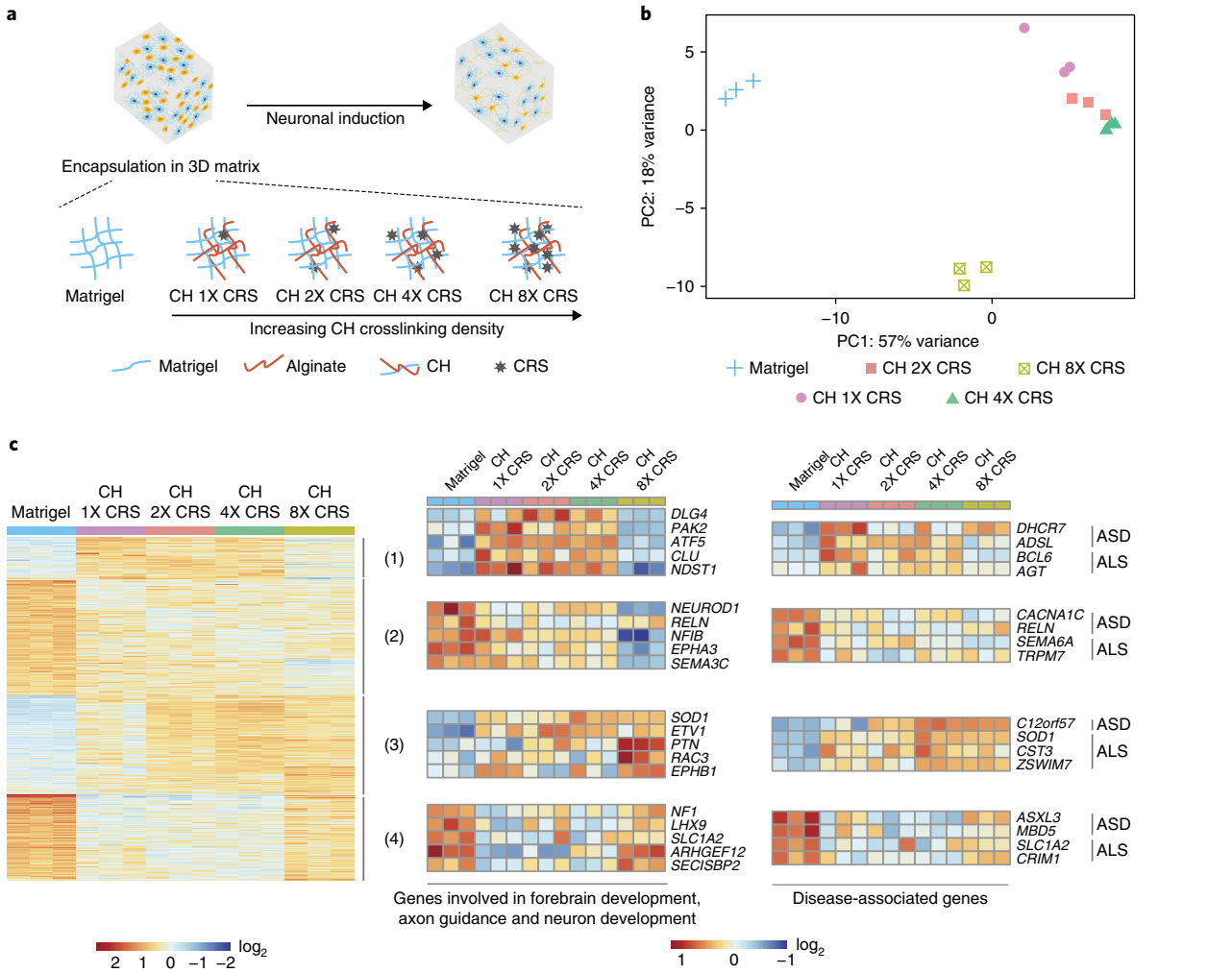

Fig. 3 | CHs modulate the expression levels of individual neuronal genes in 3D co-cultured human iN cells. a, Schematic showing human iN cells and mouse astrocytes (at a concentration of 20×10^6 cells ml^{-1}) encapsulated in Matrigel (4.6 mg ml^{-1}) or in a CH of Matrigel (4.6 mg ml^{-1}) and alginate (5 mg ml^{-1}) with varying amounts of the crosslinker (CRS) $CaCl_2$ (1X, 3.125 mM; 2X, 6.25 mM; 4X, 12.5 mM; 8X, 25 mM). **b**, PCA based on whole transcriptome data of co-cultured iN cells at week 5 of culture ($n = 3$ for each condition). **c**, Gene expression clusters for iN cells co-cultured for 5 weeks in Matrigel or CHs. Four clusters, labelled 1, 2, 3 and 4, were identified (see also Supplementary Table 5). Heatmaps show selected neuronal genes in each cluster involved in forebrain development, axon guidance and neuron development, and genes in each cluster associated with the neurological diseases ASD and ALS, and their relative expression among 3D hydrogel conditions (see also Supplementary Figs. 8, 9). Differential expression was performed between co-cultures in CH and co-culture in Matrigel with $P < 0.01$ and $\log_2$ (fold change) < -1 or $\log_2$ (fold change) > 1 used as the cut-off values.

We next compared the transcriptomes of the 3D tissues under all conditions using PCA, which showed transcriptomic differences among the various conditions (Fig. 5a). A comparison of the mechanical properties of the encapsulating hydrogels also demonstrated storage modulus differences among the various hydrogels used (Fig. 5b, Supplementary Fig. 14). We then profiled the mean correlation between the transcriptomes of the 3D tissues to the human brain transcriptome (Fig. 5c, Supplementary Fig. 15a). Moving from the Matrigel condition to the CH conditions increased the correlation to the four subregions at later developmental time points (19 and 37 pcw) while decreasing the difference between the correlations at the early developmental time point (12 pcw) and late developmental time point (37 pcw). The addition of HA to the CHs broadly decreased the correlation to the four subregions at three developmental time points (12, 19 and 37 pcw) relative to their corresponding CHs without HA. We observed the highest correlations to the four subregions at 19 and 37 pcw developmental time points with the CH with 4X crosslinker. In addition, the expression levels of a number of genes associated with neurological diseases varied across the 3D culture conditions (Fig. 5d, Supplementary Fig. 15b). These results suggest that 3D tissues could serve as substrates for studying various neurological diseases while providing transcriptomic correlations to human brain subregions at different developmental time points.

Generation of 3D neural tissues with human cell components. To better represent the cell composition of the human brain in our 3D tissues, we developed a method to derive human astrocytic cells directly from hESCs and used this method to engineer 3D tissues of co-cultured human iN and astrocytic cells. A previous study reported that overexpressing *NGN1* and *NGN2* in stem cells leads to a transient neural progenitor state before the cells turn into iN cells[18]. Thus, we hypothesized that this approach could be exploited to derive human astrocytic cells. We developed a method to induce the formation of astrocytic cells by terminating *NGN1* and *NGN2* overexpression and adding a morphogen, ciliary neurotrophic factor (CNTF), at day 2, followed by passaging the cells at day 20 to eliminate neuron-like cells (Supplementary Figs. 16a, 17).

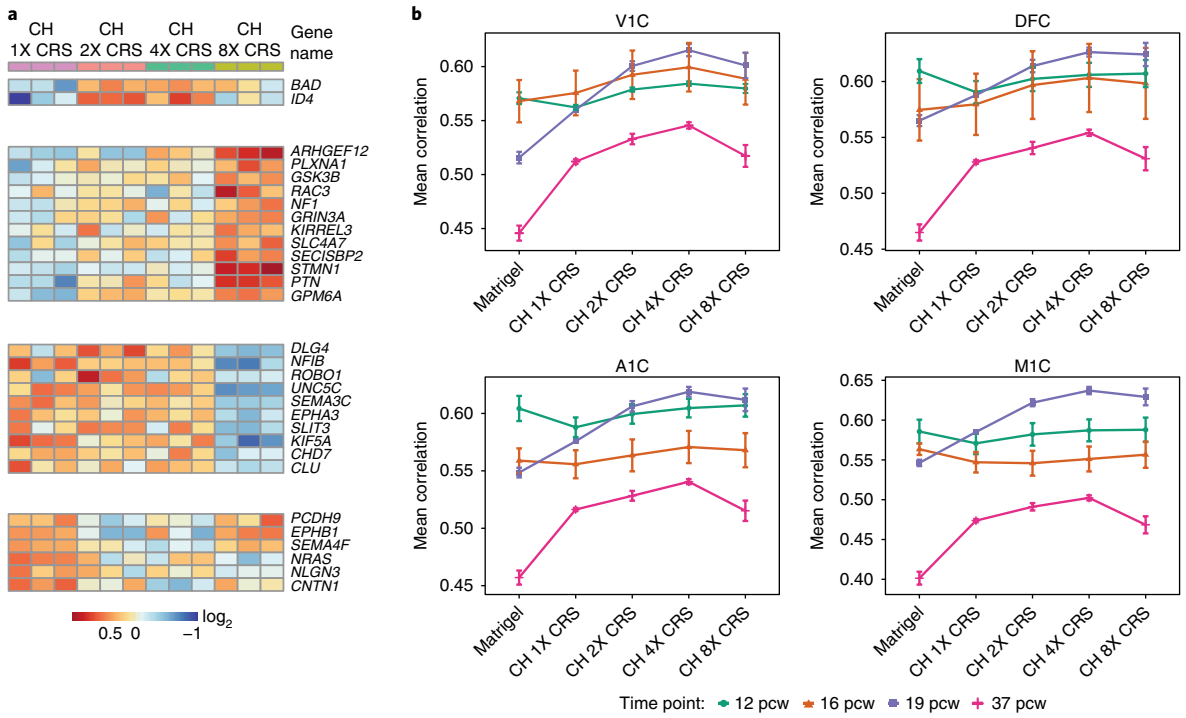

Fig. 4 | CHs alter the correlation of gene expression profiles in 3D co-cultured human iN cells to the human brain developmental transcriptome and tune the expression levels of individual neuronal genes with varying amounts of crosslinker. a, Relative expression of neuronal genes as a function of increasing amounts of the CRS $CaCl_2$ (1X, 3.125 mM; 2X, 6.25 mM; 4X, 12.5 mM; 8X, 25 mM) in the CHs (see also Supplementary Fig. 10). Differential expression was performed between co-cultures in CHs with 2X, 4X or 8X CRS and co-culture in a CH with 1X CRS, with $P < 0.05$ and $\log_2$ (fold change) < -0.75 or $\log_2$ (fold change) > 0.75 used as the cut-off values. **b**, Pearson's correlation analysis of RNA-seq data of co-cultured human iN cells in Matrigel and CHs with varying amounts of CRS compared with human brain transcriptome data of four different subregions (V1C, DFC, A1C and M1C) at four fetal developmental stages (12, 16, 19 and 37 pcw). Bars show the mean correlation ± s.e.m.

The majority of the cells thus derived were positive for GFAP, S100β and vimentin (encoded by *VIM*) at day 35, comparable to mouse astrocytes (Supplementary Fig. 18a). We also analysed the expression of *GFAP*, *S100B*, *VIM* and *ALDH1L1* by qPCR for cells exposed to different derivation protocols for 5, 15 and 30 days without passaging (Supplementary Figs. 16b, 18b). Undifferentiated hESCs, hESCs only exposed to morphogen, and human primary astrocytes were used as controls. *GFAP* expression was not detectable in undifferentiated hESCs or in hESCs only exposed to morphogen, but when morphogen was added following transcriptional activation, *GFAP* levels increased. Similarly, the expression of *S100B*, *VIM* and *ALDH1L1* gradually increased from day 5 to day 30 during the differentiation protocol (Supplementary Figs. 16b, 18b). The addition of fetal bovine serum (FBS), which is frequently used to derive astrocytes[36,37], decreased, but did not abolish, the expression of all genes tested (Supplementary Fig. 18b). However, FBS aided in the passaging steps of these cells for further expansion and was therefore included in the differentiation protocol. We also performed bulk RNA-seq throughout the course of astrocytic cell differentiation and observed that the expression levels of a number of astrocyte marker genes gradually increased starting from day 15, and by day 30 reached levels similar to that of human primary astrocytes. Moreover, these expression levels remained high at day 67 and day 114 in conditions that combined transcription activation, morphogen and FBS, whereas undifferentiated hESCs and hESCs only exposed to morphogen lacked high expression levels for the majority of astrocyte marker genes (Fig. 6a, Supplementary Fig. 18c). Consistent with our qPCR results, the addition of FBS decreased the expression levels of astrocyte marker genes at day 30, whereas expression levels of these marker genes were high at day 67 and day 114 for the same condition (Fig. 6a, Supplementary Fig. 18c). A comparison of single-cell RNA-seq (scRNA-seq) datasets of a fetal human cortex[38,39] and a single-nucleus RNA-seq dataset of an adult human brain[40] showed similar trends. That is, gradually increasing correlations of astrocytes between the adult human brain (Supplementary Fig. 19a) and the fetal human cortex (Supplementary Fig. 19c) from day 15 to day 30, particularly for conditions with transcription activation and morphogen. The addition of FBS decreased this trend (Supplementary Fig. 19a). We also analysed the expression levels of marker genes of other cell types, such as radial glia (RG), intermediate progenitor cells (IPCs), excitatory neurons and inhibitory neurons, among the samples throughout the course of astrocytic cell differentiation (Fig. 6a, Supplementary Fig. 18c). Transcriptomic correlations between these samples and corresponding cell types in fetal human cortex and adult human brain were then derived (Supplementary Fig. 19a–c). Although these comparisons suggested that there is some heterogeneity in the populations of cells arising from the astrocytic cell differentiation protocols at the transcriptomic level, the immunostaining, qPCR and RNA-seq profiles of marker genes supported the identity of these cells as astrocytic. We therefore co-cultured these cells with iN cells in a 3D system for further experiments (Fig. 6b).

To examine the impact of astrocytic cells on iN cells, we compared the gene expression profiles of iN cells co-cultured with differentiated astrocytic cells or human primary astrocytes, or cultured without astrocytic cells. We performed FACS of iN cells from all cultures at week 5 with minimal cell contamination from astrocytic cells or human primary astrocytes (Supplementary Fig. 19d,e). Gene expression profiling showed that astrocytic cells caused gene expression differences in iN cells similar to that caused by human primary astrocytes (Fig. 6c–e), providing further support that our differentiation protocol can induce astrocytic-like cell fates.

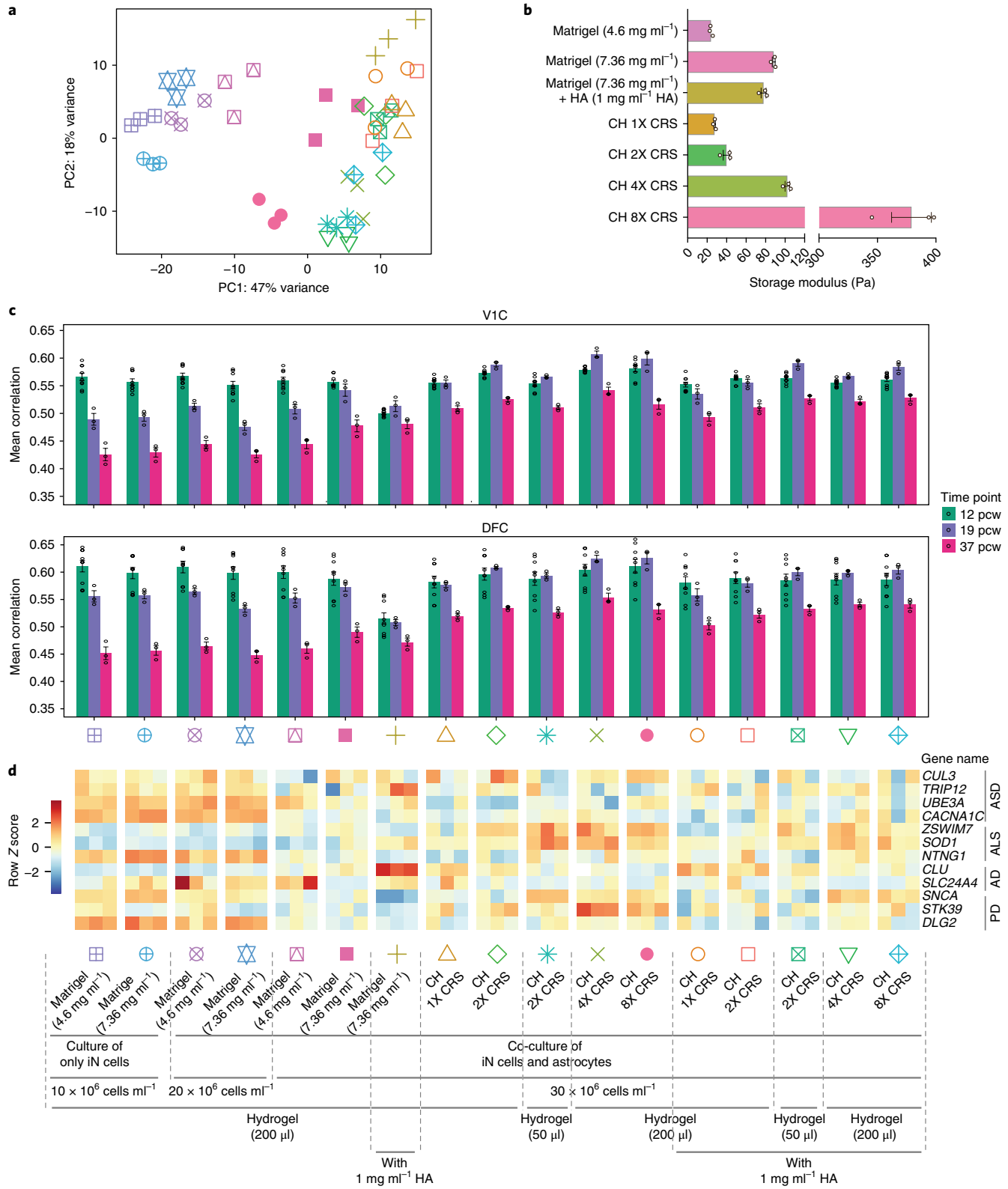

Fig. 5 | Global comparison of effects of culture conditions on human iN cells and mechanical properties of encapsulating hydrogels. a, PCA based on whole transcriptome data of iN cells cultured or co-cultured in a variety of 3D conditions at week 5 (key for the symbols are shown at the bottom of the figure) ($n = 3$ for each condition). **b**, Storage modulus at 0.5 Hz of different encapsulating hydrogels ($n = 3$ for each condition) (see also Supplementary Fig. 14). Open circles represent storage modulus values for each hydrogel condition. Bars show the mean ± s.e.m. **c**, Pearson's correlations between RNA-seq data of human iN cells cultured or co-cultured in different 3D conditions at week 5 and human brain transcriptome data of two different subregions (V1C and DFC) at three fetal developmental stages (12, 19 and 37 pcw) (see also Supplementary Fig. 15a). Open circles represent correlation values between a 3D condition and a BrainSpan sample. Each BrainSpan time point–region pair has 1 sample except for 12 pcw, which had 3 samples available for each subregion. Bars show the mean correlation ± s.e.m. **d**, Expression levels of selected disease-related genes across various 3D conditions encapsulating human iN cells (AD, Alzheimer disease; PD, Parkinson disease) (see also Supplementary Fig. 15b). Colour schemes are based on the *Z* score distribution.

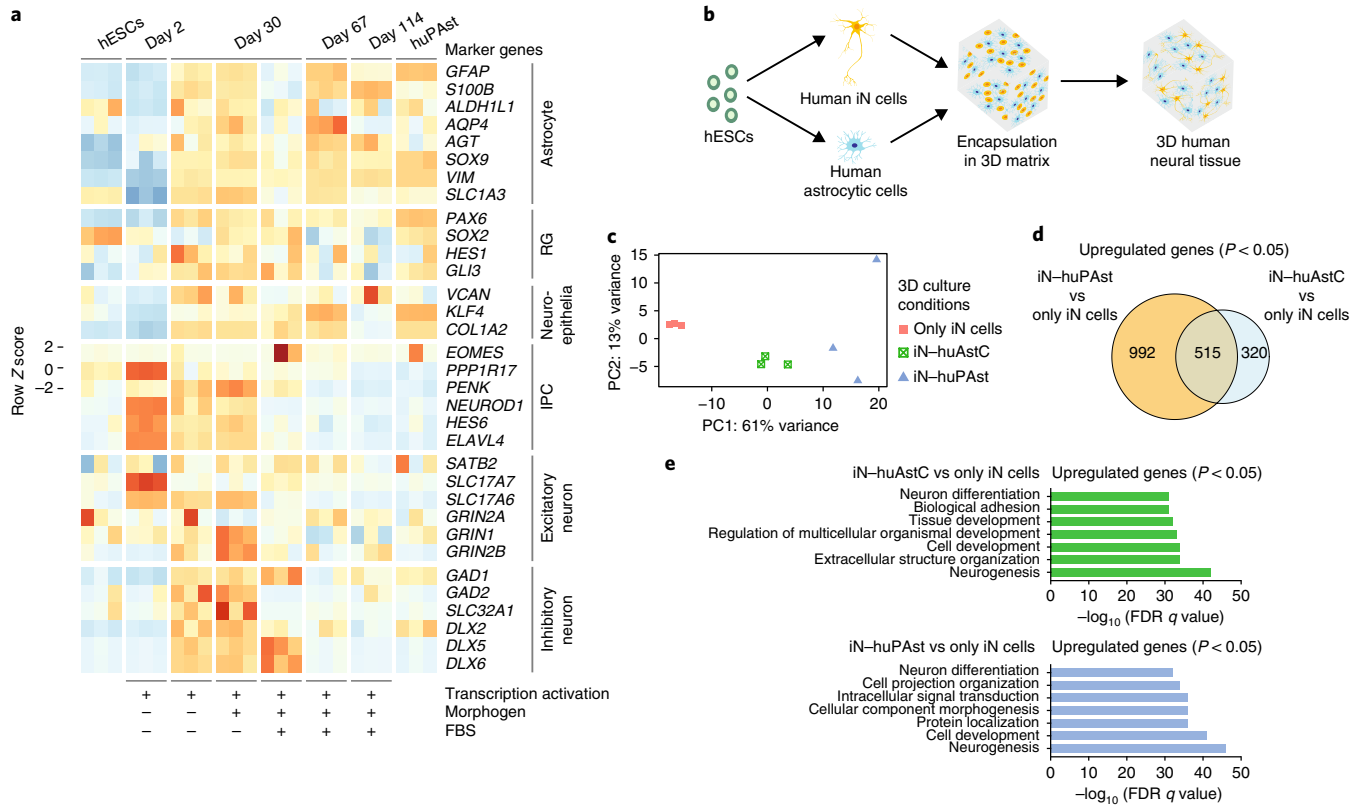

Fig. 6 | Generation of 3D neural tissues composed of human iN and astrocytic cells. a, Astrocytic cells were derived from hESCs using a combination of transcription factors used for neural induction (*NGN1* and *NGN2*), a morphogen (CNTF) and FBS. Expression levels of marker genes for a variety of cell types across different conditions of differentiation protocols at different time points. Undifferentiated hESCs were used as a negative control and human primary astrocytes (huPAst) were used as a positive control. Colour schemes are based on the *Z* score distribution ($n = 3$ for all conditions) (see also Supplementary Figs. 16, 17, 18 and 19a–c). **b**, Schematic showing the generation of 3D human neural tissues composed of human iN cells and human astrocytic cells both directly derived from hESCs. **c**, PCA based on whole transcriptome data of iN cells cultured alone or co-cultured with either human primary astrocytes (iN-huPAst) or human astrocytic cells (iN-huAstC) in Matrigel (7.36 mg ml^{-1}) at week 5 ($n = 3$ for each condition, 10^3 iN cells were sorted from each replicate for each condition) (see also Supplementary Fig. 19d,e). **d**, Venn diagram showing the number of differentially upregulated genes with $P < 0.05$ for iN-huPAst versus only iN cells and iN-huAstC versus only iN cells and the overlap of genes at week 5 (adjusted *P* value is 0.05). **e**, GO analysis for differentially upregulated genes with $P < 0.05$ for iN-huPAst versus only iN cells and iN-huAstC versus only iN cells.

To further explore the cell fates and transcriptional profiles of the cells in our tissues, we performed single-cell sequencing on 3D co-cultures of human iN cells with mouse astrocytes and with human astrocytic cells cultured in CHs with 4X crosslinker at week 5. We performed clustering on scRNA-seq profiles of human cells in both 3D co-cultures and identified 12 clusters (Fig. 7a, Supplementary Fig. 20a). Using various cell-type marker genes (Supplementary Fig. 20b–d), we classified the cell types into the following five main clusters: neurons, astrocytes, inhibitory neurons, RG, and neuroepithelia (Fig. 7b). iN cells co-cultured with mouse astrocytes contained only neuron cells (only reads aligning to the human genome were analysed), whereas iN cells co-cultured with human astrocytic cells contained cells from clusters of neurons, astrocytes, inhibitory neurons, RG and neuroepithelia (Fig. 7c), suggesting that the astrocytic cell differentiation protocol generates other transcriptionally distinct cell types in addition to astrocytes. This result was also observed in the bulk RNA-seq analysis (Fig. 6a, Supplementary Figs. 18c, 19a–c).

We next examined whether the cell-type clusters identified in our 3D tissues transcriptionally resemble their counterparts in human brain by comparing our data to scRNA-seq datasets of a fetal human cortex[38,39] and to single-nucleus RNA-seq datasets of an adult human brain[40]. Although we observed some expression of marker genes for IPCs, the transcriptomic correlation of our neuron cluster to neurons in the fetal human cortex was higher than its correlation to IPCs in the fetal human cortex (Fig. 7d,e, Supplementary Figs. 20e, 21a,b). Moreover, our neuron cluster showed a high transcriptomic correlation to different types of excitatory neurons in the fetal human cortex data, such as early- and late-born excitatory neurons in the primary visual cortex (EN-V1-2) and prefrontal cortex (EN-PFC2), and in the adult human brain (Fig. 7d,f, Supplementary Figs. 20f, 21a,b). In addition, the gene expression profile of our RG cluster correlated more with RG in the fetal human cortex, such as early RG (RG-early), dividing RG (RG-div2) and medial ganglionic eminence RG (MGE-RG2), which can give rise to inhibitory neurons[39] (Fig. 7d,e, Supplementary Figs. 20e, 21a,b). Our inhibitory neuron cluster transcriptionally correlated with both inhibitory neuron types (such as IN-CTX-MGE1; MGE-derived cortex inhibitory neurons) and excitatory neuron types identified in the fetal human cortex (Fig. 7d, Supplementary Fig. 21a,b). By contrast, in the adult human brain, the inhibitory neuron cluster correlated most highly with inhibitory neurons (Fig. 7f, Supplementary Fig. 20f). Similarly, although our astrocyte cluster correlated more highly with RG than with astrocytes in the fetal human cortex (Fig. 7d, Supplementary Fig. 21a,b), its transcriptome correlation with astrocytes in the adult human brain was higher than its correlation to other cell types (Fig. 7f, Supplementary Fig. 20f). This trend was also observed in comparisons between scRNA-seq data from 6-month-old human brain organoids[16] and scRNA-seq data from the fetal human cortex[39]

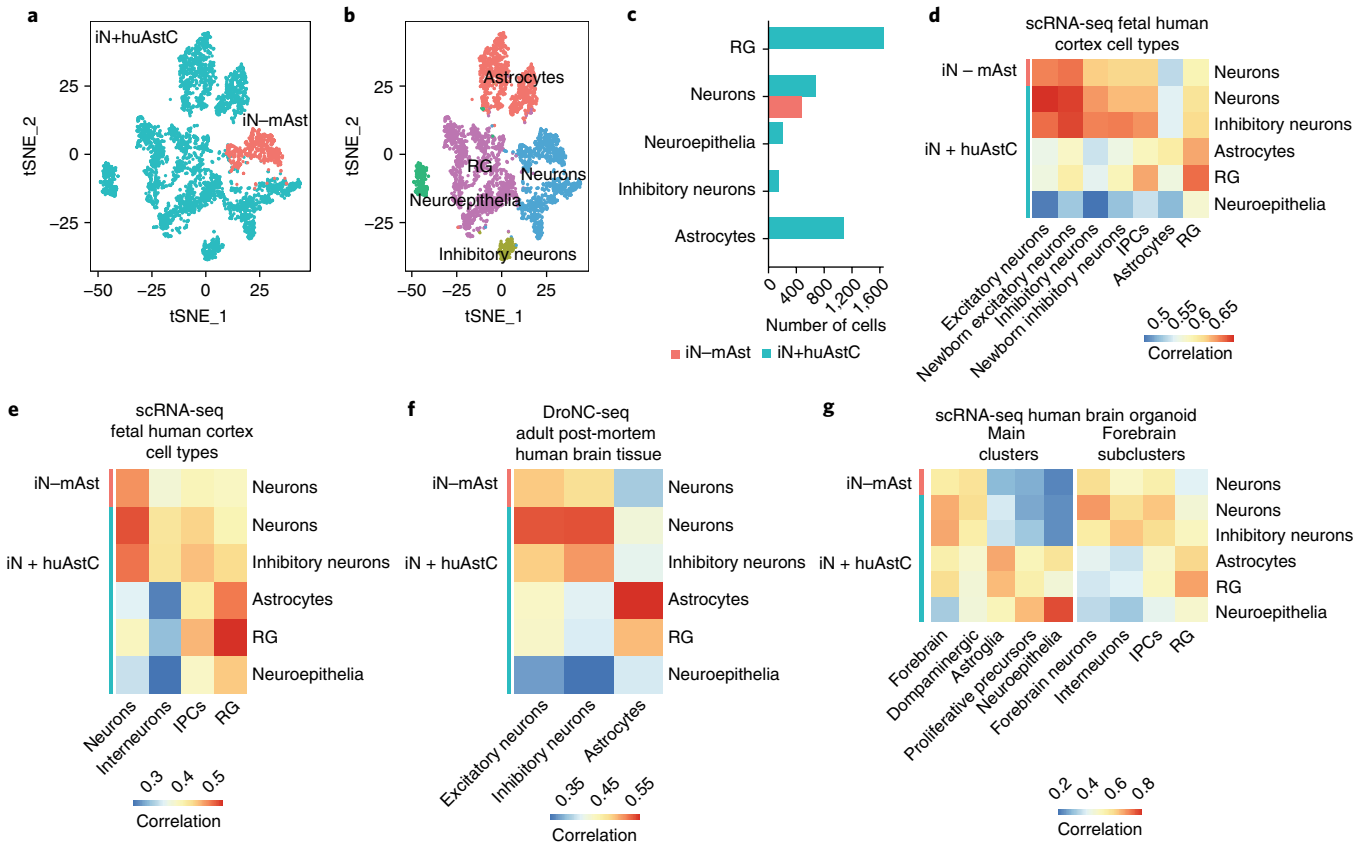

Fig. 7 | scRNA-seq reveals that cells in 3D neural tissues reflect their counterparts in the human brain and in human brain organoids. a, A t-distributed stochastic neighbour embedding (tSNE) plot of scRNA-seq profiles from iN cells co-cultured with iN–mAst and from iN cells co-cultured with iN–huAstC. Cells are coloured by condition membership. Both cultures were performed in CHs with 4X CRS ($n = 3$ for each condition). **b**,**c**, A tSNE plot showing identified clusters of distinct cell types with cells coloured by cluster membership (**b**) and number of cells in each cell type for each condition for scRNA-seq profiles shown in **a** (see also Supplementary Fig. 20) (**c**). **d**, Pearson's correlations between the average gene expression in cell type clusters shown in **b** for each condition (rows) and cell types defined by scRNA-seq in the human fetal cortex[39] (columns) (see also Supplementary Fig. 21a,b). **e**, Pearson's correlations between the average gene expression in cell type clusters shown in **b** for each condition (rows) and cell types defined by scRNA-seq in the human fetal cortex[38] (columns) (see also Supplementary Fig. 20e). **f**, Pearson's correlations between the average gene expression in cell type clusters shown in **b** for each condition (rows) and cell types (excitatory neurons, inhibitory neurons and astrocytes) defined by DroNC-seq (scRNA-seq with droplet technology) in an adult post-mortem human brain tissue[40] (columns) (see also Supplementary Fig. 20f). **g**, Pearson's correlations between the average gene expression in cell type clusters shown in **b** for each condition (rows) and main clusters and forebrain subclusters defined by scRNA-seq in 6-month-old human brain organoids[16] (columns) (see also Supplementary Fig. 20g). Forebrain subclusters were derived from a forebrain cluster shown in the main clusters.

(Supplementary Fig. 21c). To explore this result further, we performed differential expression analysis between astrocytes and RG in the scRNA-seq dataset of the human fetal cortex[39]. The top nine astrocyte-specific genes and the top nine RG-specific genes based on log fold-change (Supplementary Fig. 21d) were identified. The average expression levels of these genes in the astrocyte and RG clusters in our 3D tissues and in data from the 6-month-old human brain organoids varied among these cell types (Supplementary Fig. 21e,f). This result indicates that in both our 3D tissues and the human brain organoids, astrocytic-like cells are present but they are not transcriptionally homogeneous. Taken together, these results demonstrate that cell types in our 3D tissues transcriptionally resemble their analogues in the fetal human cortex and the adult human brain. Finally, a comparison between scRNA-seq profiles of our 3D tissues and the scRNA-seq dataset of 6-month-old human brain organoids[16] revealed that the transcriptomes of our cell-type clusters correlated with their counterparts in 6-month-old human brain organoids (Fig. 7g, Supplementary Fig. 20g).

As a proof-of-concept, we tested the feasibility of performing CRISPR (clustered regularly interspaced short palindromic repeats)-mediated genome editing in our engineered 3D neural tissues in a disease context. Using Cpf1-mediated genome editing via adeno-associated virus (AAV)-based gene delivery[41,42], we targeted *SOD1*, *TARDBP* and *TBK1*, genes implicated in ALS and frontotemporal dementia[43–46]. We identified insertions and deletions (indels) in three independently targeted loci and found ~5%, ~14% and ~6% indel formation in *SOD1*, *TARDBP* and *TBK1*, respectively (see Supplementary Text, Supplementary Figs. 22, 23). These results show that our 3D human neural tissue system can be combined with genome editing and gene delivery tools to perturb genes implicated in neurodegenerative diseases.

Discussion

3D neural tissues have the potential to be tractable models for studying the human brain and neurological disorders, but to achieve this potential, they must closely reflect the cell composition, ECM and gene expression profiles of the human brain. Here, we analysed how the transcriptome of iN cells in 3D tissues relates to the human brain transcriptome and is affected by a number of tissue engineering variables. Furthermore, we developed an approach

to generate co-cultured iN and astrocytic cells derived from hESCs in a 3D matrix that can be tuned to reflect different transcriptomic states of the human developing brain transcriptome, which will be helpful for rapidly generating complex neurological disease models.

To gain a global view of the brain-like properties of these engineered tissues, we compared the transcriptomes of cells grown in 3D cultures with those grown in 2D cultures. We found more enriched neuronal biological processes in iN cells cultured in 3D Matrigel than those grown in 2D cultures (Fig. 1f), and this result was not affected by batch-to-batch variations in Matrigel (Supplementary Fig. 3a–c). In addition, transcriptome profiling showed enriched apoptotic and oxidative stress biological processes in cells grown in 2D cultures compared with those grown in 3D cultures, and 3D cultures enabled electrophysiological measurements (Supplementary Figs. 2, 4). These results suggested that iN cells in 3D cultures were healthier than cells in 2D cultures, although we did not directly test cell viability. In addition, we co-cultured iN cells with mouse astrocytes both in 3D and on 2D systems. Although iN cells in both co-cultures were electrophysiologically active at later time points, the transcriptome of 3D co-cultured iN cells was more enriched in neuronal biological processes than that of 2D co-cultured iN cells, indicating that 3D tissues offer a closer approximation to biology than 2D tissues. Varying the cell seeding densities or independent components of the encapsulating matrix (for example, laminin, collagens or synthetic hydrogels) may lead to different characteristics of the iN cells, avenues that could be explored in future functional studies.

Engineered neural tissues can be made more brain-like by adding other ECM components, such as HA, which has been shown to promote better replication of the brain microenvironment[29–31]. Under the conditions we tested, however, the incorporation of HA in our 3D Matrigel co-cultures of iN cells did not strongly improve the correlation to the transcriptome of the human developing brain, although some individual neuronal transcripts and genes associated with neurological diseases were upregulated (Fig. 5, Supplementary Fig. 7b). We chose to use a high molecular mass HA and incorporated it in a high concentration of Matrigel (which showed a storage modulus closed to Matrigel without HA due to the uncrosslinked state of HA in Matrigel) to minimize its diffusion from the hydrogel structures while maintaining its natural state[26,28]. However, other variables (such as chemical modifications and the concentration and source of HA[47,48]) or shorter culture times (such as 1 week) that were not tested may have a greater impact on gene expression. Given that high molecular mass HA is thought to inhibit remyelination following central nervous system injury[26,49], introducing HA into hydrogels could impede the expression of genes involved in neuronal development.

Matrix stiffness in engineered tissues can also affect cellular properties and can be increased in a pure Matrigel hydrogel simply by increasing the concentration of Matrigel[33,50]. Alternatively, in a CH, stiffness can be increased by increasing the amount of crosslinker while maintaining the concentration of alginate and Matrigel constant[33]. We therefore investigated whether developing 3D co-cultures of iN cells within CHs of Matrigel and alginate improved the transcriptomic correlation to human brain samples. Alginate is a naturally occurring polysaccharide composed of mannuronic acid and guluronic acid with no cell adhesion ligands, and can be crosslinked to form a network within Matrigel through the addition of divalent cations such as calcium[33]. We demonstrated that increasing the crosslinking of the alginate network in CHs (which led to an increased storage modulus) can tune the correlation of the transcriptome of 3D co-cultured iN cells to the transcriptome of particular subregions of the human brain at specific developmental stages. Furthermore, modulating the amount of crosslinker and/or the volume of the CH led to gene expression changes in specific neuronal transcripts, including *DLG4*, *GRIN3A* and *SOD1*, as well as changes in the expression levels of genes associated with neurological diseases (Figs. 3c, 5d). As HA has been previously integrated in crosslinked alginate hydrogels[51], we incorporated HA in CHs of Matrigel and alginate and, in agreement with our other results, found it had little effect. It will be informative to analyse the effects of changing the hydrogel volume or removing the Matrigel on the cellular state to better understand how these parameters affect gene expression.

To better model the cell composition in the human brain within our 3D tissues, we first developed a method to derive human astrocytic cells directly from hESCs. We exploited a previously reported transient neural progenitor state of stem cells induced via the overexpression of neurogenins[18] to differentiate cells towards an astrocytic phenotype. Immunostaining, qPCR and bulk RNA-seq analyses showed that the derived astrocytic cells expressed astrocyte markers and that this expression increased over time. By day 15, we could detect the expression of marker genes for astrocytic cells, inhibitory neurons and RG, thus demonstrating the potential for rapidly creating 3D tissues with controlled composition of these cell types by generating reporter cell lines using these markers. Using scRNA-seq, we evaluated the gene expression profiles of the cells arising from our differentiation protocols and compared these to published transcriptional datasets of fetal and adult human brain as well as human brain organoids. We found that the cells present in our 3D co-cultured tissues broadly reflected their counterparts in the human brain, and we observed interesting similarities between the gene expression profiles in our system and in human brain organoids as they relate to the human brain data. Overall, these results suggest that we were able to generate relevant cell types, but further functional studies are required to fully characterize these astrocytic cells and inhibitory neurons in our system. Moreover, it will be informative to test additional differentiation protocols (such as the use of other transcription factors or small molecules) to further expand the cells types that can be studied in this system.

Our method of deriving both iN and astrocytic cells from the same pool of hESCs enables the rapid creation of engineered tissues with an isogenic background. These 3D tissues, composed of iN cells (at day 35) and astrocytic cells (at day 118), exhibited transcriptional profiles that correlated with relevant cell types in the human brain as well as with 6-month-old human brain organoids, suggesting that this system may be a faster alternative to organoids. To demonstrate the potential for studying the genetics of neurodegenerative diseases in our 3D neural tissues, we perturbed three genes implicated in ALS and frontotemporal dementia using Cpf1[52] directly in iN cells, and observed at least 5% indel formation rates for each gene. Directly injecting AAV mixtures within 3D tissues instead of mixing with culture medium could be tested in future studies to improve indel formation rates. This approach could be extended by independently targeting astrocytic cells within 3D tissues by using the *GFAP* promoter in gene editing constructs.

Despite the potential for this approach as a scalable method for interrogating the genetics of brain disorders, there are a number of limitations and challenges. All 3D tissue models are limited in their ability to recapitulate complex environmental features, such as the interplay between the immune system and the central nervous system, vasculature and the signals that are distributed throughout this network, and ageing. Nevertheless, as the technology and our understanding of the brain advances, it should be possible to develop increasingly complex tissues that contain multiple cell types that develop over time.

Outlook

By varying the parameters of the 3D neural matrix (for example, adjusting the composition), we have shown that our engineered tissues can be tuned to express different levels of neuronal transcripts as well as genes associated with neurological diseases and to reflect specific stages of the human brain developmental transcriptome.

Single-cell sequencing revealed that our 3D tissues contain cell types that transcriptionally resemble their analogues in the human brain, further supporting the utility of this system. In combination with genome editing tools, which can be used to precisely disrupt specific genes in a cell-type specific manner, these tissues offer an adaptable and genetically tractable system for studying neurological disorders. In particular, the ability to rapidly model polygenic diseases such as ALS, Alzheimer disease and Parkinson disease in a controllable environment will be particularly beneficial for unravelling these complex diseases. This goal may be achieved by either independently targeting gene function in neuronal and astrocytic cells or developing 3D tissues directly from hESCs carrying the desired mutations and utilizing scRNA-seq[53,54] or single-nucleus RNA-seq[40] methodologies in combination with functional studies. The analyses described in this study and continued interrogation of 3D culture systems will further aid the development of more effective models for brain diseases.

Methods

hESC culture. The hESC line HUES66 was obtained from the Harvard Stem Cell Institute (cells were not re-identified or tested for mycoplasma contamination). Stem cells were cultured in 10 cm tissue culture dishes coated with 5 ml of Geltrex (Thermo Fisher Scientific) diluted in DMEM (Thermo Fisher Scientific) at 1:100 ratio and incubated for 30 min at 37 °C. Stem cell culture medium contained mTeSR (Stemcell Technologies), the supplement provided with mTeSR and normocin (InvivoGen). Stem cells were passaged by detaching with Accutase (Stemcell Technologies) diluted in DPBS (Thermo Fisher Scientific) at a ratio of 1:3. After each splitting of stem cells, 10 μM of Rho-associated kinase (ROCK) inhibitor (EMD Millipore) was added in medium of re-plated cells. Stem cell culture medium was replaced daily.

Generation of iN cells from hESCs. To produce iN cells, hESCs were infected with lentiviral vectors. These vectors provided constitutive expression of *rtTA3* driven by the human *EF1A* promoter, and doxycycline-inducible expression of human *NGN1* and *NGN2* driven by the *TRE* promoter. The puromycin-resistant gene was linked to *NGN1* and *NGN2* by a P2A linker to enable selection. Lentivirus-infected hESCs were plated at ~15×10^3 cells cm^{-2} in 15 cm tissue culture dishes pre-coated with 10 ml of growth factor reduced (GFR) Matrigel (Corning) (at 8.5 mg ml^{-1} to 10 mg ml^{-1} concentration) diluted in DMEM at 1:100 and incubated for 30 min at 37 °C. Day 0 medium of plated stem cells contained stem cell culture medium and 2 μg ml^{-1} doxycycline (Sigma) to initiate expression of *NGN1* and *NGN2*. The entire medium at day 1 was replaced by medium containing 3 volumes of stem cell culture medium and 1 volume of neural culture medium along with 2 μg ml^{-1} doxycycline and 1 μg ml^{-1} puromycin. Neural culture medium was prepared by mixing 500 ml of neurobasal medium (Thermo Fisher Scientific), 10 ml of B27 supplement (Thermo Fisher Scientific), 5 ml of penicillin–streptomycin (Thermo Fisher Scientific) and 5 ml of Glutamax (Thermo Fisher Scientific). On day 2, the entire medium was replaced by medium made of 1:1 mixture of stem cell culture medium and neural culture medium, and 2 μg ml^{-1} doxycycline and 2 μg ml^{-1} puromycin were added into culture medium. On day 3, iN cells were ready for detachment and growth in 2D or in 3D culture conditions.

Primary mouse glia culture. Mouse glial cells were isolated from the cortices of newborn C57 mice in procedures carried out in accordance with the Animal Care and Use regulations at the Broad Institute, with the protocol (0008-06-14) approved by the Broad Institute's Institutional Animal Care and Use Committee (IACUC). Cortices of newborn mice were dissected and digested using papain for 30 min and applying agitation. Dissociated cells were plated in tissue culture dishes in DMEM supplemented with 10% FBS. Glial cells were passaged by trypsinizing and replating at lower density more than eight times to remove the potentially low amounts of mouse neurons in culture before their use in 2D and 3D co-cultures with iN cells.

2D cultures and co-cultures of iN cells. For 2D cultures of iN cells, 5 glass coverslips (Corning-Biocoat) were inserted per well of a 6-well plate. Then, each well with coverslips was coated with 1.5 ml of GFR Matrigel diluted in DMEM at 1:100 and incubated for 30 min at 37 °C. The coating solution was aspirated from each well before cell seeding. iN cells generated within 3 days as described above were detached from culture plates using Accutase diluted in DPBS at 1:3. iN cells were seeded on each pre-coated well with coverslips at 50×10^3 cells cm^{-2} in 3 ml medium made of a 1:3 mixture of stem cell culture medium and neural culture medium (hereafter, termed 1:3 culture medium) with 2 μg ml^{-1} doxycycline. One day later, the entire medium of each well was replaced with 3 ml neural culture medium with 2 μg ml^{-1} doxycycline. On the second day of seeding, 1 ml of neural culture medium with doxycycline and Ara-C was added in each well, keeping the final concentration of doxycycline in each well at 2 μg ml^{-1} and the final concentration of Ara-C in each well at 0.5–1 μM. One-third of the entire culture medium in each well was replaced every 3–4 days. For 2D co-cultures of iN cells with mouse glia, 6-well plates with coverslips were prepared as described above. Mouse astrocytes were detached from culture plates using trypsin. iN cells and mouse glia were mixed 1:1 and seeded on each pre-coated well with coverslips at 100×10^3 cells cm^{-2} in 3 ml 1:3 culture medium with 2 μg ml^{-1} doxycycline. For the rest of the culture, the protocol was performed as described above, except that the final concentration of Ara-C in each well was at 2–5 μM, which was added with the neural culture medium in each well on the second day of seeding.

3D cultures and co-cultures of iN cells. 3D cultures and co-cultures of iN cells were performed by encapsulating them within hydrogels. These hydrogels were made of pure GFR Matrigel, GFR Matrigel and HA, GFR Matrigel and alginate, or GFR Matrigel, alginate and HA. Before the encapsulation experiments, the following preparations were performed: GFR Matrigel was kept on ice, sodium alginate (PRONOVA UP VLVG, NovaMatrix) was first reconstituted at 4% (40 mg ml^{-1}) in a medium made of a 1:3 mixture of mTeSR and neurobasal medium (without supplements) with 150 mM sodium chloride (Sigma) and this solution was then incubated for 6 h at 37 °C to enable further dissolution of the alginate. This alginate stock solution was passed through a 0.22 μm filter (EMD Millipore) and kept on ice. Calcium chloride ($CaCl_2$) solution (1 M in water, Sigma) was diluted in a medium made of a 1:3 mixture of mTeSR and neurobasal medium (without supplements) at concentrations of 25 mM, 12.5 mM, 6.25 mM and 3.125 mM. These $CaCl_2$ solutions were individually passed through 0.22 μm filters and kept on ice. HA sodium salt (Sigma, #53747) was dissolved at 1% (10 mg ml^{-1}) concentration under sterile conditions in a medium made of a 1:3 mixture of mTeSR and neurobasal medium (without supplements) and then incubated for 6 h at 37 °C to enable further dissolution of the HA and frequently vortexed. This HA stock solution was kept on ice. A sheet of Parafilm and a microcentrifuge tube rack were sprayed with 70% ethanol and kept in a biohood under UV light for 30 min. Parafilm dimples were formed by placing a sheet of Parafilm on the microcentrifuge tube rack and pressing gently on Parafilm. Serum-free DMEM was kept on ice.

3D cultures of iN cells were performed by encapsulating them within 200 μl hydrogels of Matrigel at 10×10^6 cells ml^{-1}. iN cells generated within 3 days were detached as previously described and filtered through a 40 μm cell strainer (Corning), and pelleted at the desired amount. The final concentration of encapsulating Matrigel was either 4.6 mg ml^{-1} or 7.36 mg ml^{-1}. As the Matrigel stock concentration varied from batch to batch (8.5 mg ml^{-1} to 10 mg ml^{-1}), different amounts of 1:3 culture medium were used to adjust the final concentration of Matrigel in hydrogels and kept on ice until used. A desired amount of Matrigel stock was placed in a 1.5 ml centrifuge tube and kept on ice. A pipette tip was chilled by pipetting cold serum-free DMEM. This pipette tip was then used to resuspend the iN cell pellet in pre-chilled 1:3 culture medium. These resuspended iN cells were then mixed with the Matrigel in the 1.5 ml centrifuge tube. The final concentration of iN cells in this cell–gel solution was 10×10^6 cells ml^{-1}, and the final concentration of Matrigel in this solution was either 4.6 mg ml^{-1} or 7.36 mg ml^{-1}. The cell–gel solution was vortexed for 10 s and then kept on ice while chilling a pipette tip by pipetting cold, serum-free DMEM. This pipette tip was then used to place 200 μl droplets of cell–gel solution one by one on the Parafilm dimples. These droplets were then placed at 37 °C for 1 h to allow gelation of the Matrigel. Each droplet was subsequently placed in one well of a 6-well plate by gently pipetting it from the Parafilm with 1 ml of 1:3 culture medium with 6 μg ml^{-1} doxycycline. After placing all the droplets in the culture plate, 2 ml of the same culture medium was added to each well. At day 1, the entire medium of each well was substituted with 3 ml neural culture medium containing 6 μg ml^{-1} doxycycline. On the second day of encapsulation, 1 ml neural culture medium with doxycycline and Ara-C was added to each well, ensuring that the final concentration of doxycycline in each well was 6 μg ml^{-1} and the final concentration of Ara-C in each well was 0.5–1 μM. One-third of the entire culture medium in each well was renewed every 3–4 days.

3D co-cultures of iN cells with mouse astrocytes were carried out by encapsulating them within 200 μl hydrogels made of either Matrigel (either 4.6 mg ml^{-1} or 7.36 mg ml^{-1}) or Matrigel and HA (7.36 mg ml^{-1} Matrigel and 1 mg ml^{-1} or 1.5 mg ml^{-1} final HA concentration) or CHs (4.6 mg ml^{-1} Matrigel and 0.5% final concentration of alginate, with and without HA). iN cells were prepared as described above. Mouse astrocytes were detached by trypsinizing and filtered through a 40 μm cell strainer, and pelleted at the desired amount. All hydrogels contained 1:1 mixture of iN cells and mouse astrocytes. For pure Matrigel hydrogels, the cell concentration was either 20×10^6 cells ml^{-1} or 30×10^6 cells ml^{-1}. For hydrogels of Matrigel and HA, the cell concentration was 30×10^6 cells ml^{-1}. Different amounts of 1:3 culture medium were used to adjust the final concentration of Matrigel and HA in hydrogels and kept on ice until use. Tissues were prepared as described above with the following additions: for hydrogels of Matrigel and HA, a desired volume from 1% HA stock was pipetted in Matrigel in the tube to a final concentration of HA at either 1 mg ml^{-1} or 1.5 mg ml^{-1}. Cell suspensions were then mixed either with pure Matrigel or with a mixture of Matrigel and HA in the centrifuge tube. For CHs, the cell concentration within hydrogels was either 20×10^6 cells ml^{-1} or 30×10^6 cells ml^{-1}.

For CHs containing HA, the cell concentration was 30×10^6 cells ml^{-1}. $CaCl_2$ was used to crosslink alginate in the CHs. Each 200 µl droplet of CH was made by mixing 150 µl cell–gel solution with 50 µl $CaCl_2$ solution on a Parafilm dimple. The cell–gel solution was prepared accordingly so that in each 200 µl CH, the final concentration of Matrigel was 4.6 mg ml^{-1} and that of alginate was 0.5%. For each 200 µl droplet of CH containing HA, the final HA concentration was either 1 mg ml^{-1} or 1.5 mg ml^{-1}. To prepare gel solutions, a desired volume of Matrigel was placed in a centrifuge tube with a pre-chilled pipette tip and then the desired volume of 4% alginate was mixed with Matrigel in the centrifuge tube with a pre-chilled pipette tip, vortexed for 10 s, and kept on ice. For CHs containing HA, a desired volume of 10 mg ml^{-1} HA was mixed with Matrigel and alginate solution, vortexed for 10 s, and kept on ice. A volume of 1:3 culture medium required to adjust the concentration of components in gel solution was used to resuspend 1:1 mixture of iN cells and mouse astrocytes. These resuspended cells were then mixed with gel solutions and vortexed for 10 s. Each 200 µl droplet of CH was made by first placing 50 µl $CaCl_2$ solution (at concentrations of 25 mM, 12.5 mM, 6.25 mM and 3.125 mM) on a Parafilm dimple and then rapidly mixing 150 µl cell–gel solution with this $CaCl_2$ solution on a Parafilm dimple with a pre-chilled pipette tip without generating bubbles. Droplets (50 µl) of CHs were generated in the same manner by adjusting volumes. To allow Matrigel gelling, all droplets were then placed at 37 °C for 1 h. After forming the hydrogels, the same protocol as described above was followed for the remainder of the experiment, except the final concentration of Ara-C in each well was at 2–5 µM, which was added with the neural culture medium in each well on the second day of encapsulation.

3D and 2D cultures of iN cells with two different batches of Matrigel. For 2D cultures of iN cells, independent wells of a 6-well plate with coverslips were coated with two different batches of Matrigel, and iN cells were seeded on each pre-coated well with coverslips at 50×10^3 cells cm^{-2}. 3D cultures of iN cells were performed by encapsulating them within separate 200 µl droplets of hydrogels of 4.6 mg ml^{-1} Matrigel from two different batches at 10×10^6 cells ml^{-1}. Protocols for 3D and 2D cultures of iN cells described above were subsequently followed.

Rheolological measurements. Hydrogels (100 µl volume) without cells were formed as described above. The mechanical properties of the hydrogels were characterized using a AR 2000 rheometer (TA Instruments) fitted with a Peltier stage set to 37 °C. Oscillatory frequency sweep measurements were conducted at a 0.5% strain amplitude. All measurements were performed in triplicate using a 8 mm 4° cone and 200 µm gap size, and the results analysed using TRIOS software (TA instruments).

Derivation of human astrocytic cells. Each well of a 6-well plate was coated with 1.5 ml of GFR Matrigel diluted in DMEM at 1:100 ratio and incubated for 30 min at 37 °C. Lentivirus-infected hESCs containing inducible expression constructs of *NGN2* and *NGN1* were plated at ~15×10^3 cells cm^{-2} in pre-coated wells. Expansion medium was prepared by mixing 500 ml of DMEM, 10 ml of N2 supplement (Thermo Fisher Scientific), 5 ml of penicillin–streptomycin and 5 ml of Glutamax. Day 0 medium of plated stem cells contained stem cell culture medium (as previously described), 2 µg ml^{-1} doxycycline to initiate expression of *NGN2* and *NGN1*, and 10 µM ROCK inhibitor. At day 1, the entire medium in each well was replaced by medium containing 3 volumes of stem cell culture medium and 1 volume of expansion medium along with 2 µg ml^{-1} doxycycline and 2 µg ml^{-1} puromycin. At day 2, for the sample termed "unconditioned" (Supplementary Fig. 16a), the entire medium was replaced by expansion medium, and for the sample termed "morphogen", the entire medium was replaced by expansion medium with 15 ng ml^{-1} CNTF. At day 4, half of the medium in each well for both conditions was renewed with their corresponding culture medium. At day 5, for the unconditioned sample, one-third of the entire culture medium was replaced with expansion medium, whereas for the morphogen sample, one-third of the entire culture medium was replaced with expansion medium with 15 ng ml^{-1} CNTF. For the sample termed "morphogen + FBS", one-third of the entire culture medium was replaced with expansion medium with 1% FBS and 15 ng ml^{-1} CNTF. One-third of the entire culture medium of all conditions was replaced with their corresponding medium every 4–5 days.

At day 20, cells in all conditions were passaged and seeded back in wells pre-coated as described above. The morphogen + FBS cells were expanded for further use in generating 3D human neural tissues by co-culturing them with iN cells in a matrix. The morphogen + FBS cells at day 35 were used for immunostainings.

For control experiments, lentivirus-infected hESCs were seeded as previously described and treated using the morphogen protocol for 30 days without including the application of doxycycline and puromycin. In addition, lentivirus-infected hESCs cultured in stem cell culture medium without and not subjected to the differentiation protocol were used as a control. Human primary astrocytes (ScienCell) were cultured in expansion medium with 2% FBS and used as a control. For qPCR experiments for astrocytic cells, the protocol for all conditions was continued without passaging cells, except for human primary astrocytes, which were in passage 3. For RNA-seq experiments for astrocytic cells, the protocol for all conditions was continued without passaging cells, except for the morphogen + FBS condition, samples at day 67 were in passage 3 and samples at day 114 were in passage 6, and human primary astrocytes were in passage 3. RNA lysis buffer (Zymo Research) was used to lyse cells in each well for all conditions.

3D co-cultures of iN cells with human astrocytic cells and with human primary astrocytes. Astrocytic cells derived following the morphogen + FBS protocol cultured until day 52 (passage 5) and day 61 (passage 7) were detached from culture plates with Accutase and pooled for 3D cultures and co-cultures with iN cells. For 3D co-cultures of iN cells with human astrocytic cells, a 1:1 mixture at a final cell concentration of 20×10^6 cells ml^{-1} were encapsulated in 100 µl of hydrogels (7.36 mg ml^{-1} Matrigel). 3D co-cultures of iN cells with human primary astrocytes (passage 5) were carried out by encapsulating a 1:1 mixture (at a final cell concentration of 20×10^6 cells ml^{-1}) within 100 µl of hydrogels (7.36 mg ml^{-1} Matrigel). 3D cultures of iN cells alone and 3D cultures of human astrocytic cells alone were performed by encapsulating them (at a final cell concentration of 10×10^6 cells ml^{-1}) within separate 100 µl of hydrogels (7.36 mg ml^{-1} Matrigel). After encapsulations, culture protocols as described above were followed but with the following changes: the culture medium did not contain doxycycline and the final concentration of Ara-C in each culture well was 1 µM. Six days after the formation of 3D cultures and co-cultures, the 3D cultures and co-cultures of iN cells were infected with AAV U6-hSyn1-mCherry-KASH-hGH vectors encoding non-targeting single guide RNA to enable FACS of iN cells. At week 5 of culture, 3D cultures and co-cultures of iN cells were disassociated by first individually immersing 3D tissues in Accutase, incubating at 37 °C for ~8 min, and then disrupting the 3D matrix by pipetting in Accutase. Each disassociated tissue sample was resuspended in neural culture medium and centrifuged at 200 *g* for 5 min. Each pellet was then resuspended in DPBS and passed through a 30 µm filter (Sysmex) to remove potential cell clumps and hydrogel residue before cell sorting. Cell suspensions were sorted using a Beckman Coulter MoFlo Astrios EQ cell sorter (Broad Institute Flow Cytometry Core). Each 3D culture and co-culture was analysed in triplicate, and a population of 1×10^3 mCherry-positive iN cells was collected from each disassociated 3D tissue into DNA/RNA Shield (Zymo Research). 3D cultures of human astrocytic cells were individually immersed in DNA/RNA Shield without cell sorting.

RNA isolation. For 2D cultures of iN cells and their 2D co-cultures with mouse astrocytes and for 2D cultures of only mouse astrocytes, 2D cultured hESCs, and day 3 iN cells, 300 µl of RNA lysis buffer (Zymo Research) was used to lyse cells in each well of a 6-well plate. Each lysate was then transferred to a 1.5 ml centrifuge tube. For 3D cultures of iN cells and their 3D co-cultures with mouse astrocytes, each hydrogel was transferred using an RNase-free spatula (Corning) from a culture well to a 1.5 ml centrifuge tube and immersed in 300 µl of RNA lysis buffer. All centrifuge tubes were placed on dry ice for rapid freezing and then stored at −80 °C. Total RNA isolation was performed using a Zymo RNA QuickPrep Mini kit (Zymo Research) following the manufacturer's protocol with the following modifications. 3D culture hydrogels were homogenized using a hand-held pestle (Fisher Scientific) in a 1.5 ml Eppendorf tube containing 300 µl lysis buffer with a few strikes to break down the large pieces. Lysates were transferred to a ZR BashingBead Lysis Tube (Zymo Research) and bead bashed on a D2400 Homogenizer (BenchMarker) for 45 s at full speed 7. After 1 min of centrifugation at 14,000 *g*, supernatant was recovered and used for RNA isolation using a standard procedure. For CH 3D cultures, another purification step was performed on the eluted RNA samples using 1.8 times volumes of RNAClean SPRI beads (Agencourt). For conditions involved in the derivation of astrocytic cells, conditions in 3D cultures and co-cultures of iN cells with human astrocytic cells and with human primary astrocytes, and 3D cultures of human astrocytic cells, a Zymo RNA QuickPrep Mini kit (Zymo Research) was used to isolate the total RNA by following the manufacturer's recommended protocol.

RNA-seq. RNA-seq libraries were prepared following the Smart-seq2 protocol[55] with the following modifications: 1 ng of total RNA was used in place of a single cell lysate. For 2D and 3D cultures of iN cells, 3D co-cultures of iN cells with mouse astrocytes, 2D cultured hESCs, and day 3 iN cells, 12 cycles of PCR were used to amplify the cDNA, and 0.25 ng of amplified cDNA was used in each NexteraXT (Illumina) reaction. For 2D co-cultures of iN cells with mouse astrocytes, 2D cultures of mouse astrocytes, samples in astrocytic cell differentiation protocols, 3D co-cultures of iN cells with differentiated astrocytic cells and with human primary astrocytes, and 3D cultures of iN cells alone, 12 cycles of PCR were used to amplify the cDNA, and 0.075 ng of amplified cDNA was used in each NexteraXT (Illumina) reaction. For samples in the Matrigel batch tests, 15 cycles of PCR were used to amplify the cDNA, and 0.075 ng of amplified cDNA was used in each NexteraXT (Illumina) reaction. Pooled libraries were sequenced on a NextSeq 500 instrument (Illumina) with 50 bases for read1 and 25 bases for read2.

Transcriptome analyses. RSEM v.1.3[56] was run on fastq files of cultures of iN cells and their co-cultures with mouse astrocytes using a joint human (hg19 annotation from UCSC) and mouse (mm10 annotation from UCSC) transcriptome and STAR v.2.5.2[57], with the options --star --star-gzipped-read-file --paired-end. The count data output by RSEM was used to quantify the percentage mouse reads versus the

percentage human reads. The STAR bams output by RSEM were used to filter the original fastq files with seqtk (https://github.com/lh3/seqtk). In particular, all reads that mapped to the mouse transcriptome were removed, as were all unmapped reads. These filtered fastq files were run through RSEM with default parameters using the human hg19 UCSC genome to estimate gene expression values, which were then used to create an non-normalized count matrix. This count matrix was used for further analysis involving co-culture conditions of iN cells with mouse astrocytes. For the data analysis of culture conditions of iN cells without mouse astrocytes, RSEM with default parameters was run on fastq files of cultures of iN cells using the human hg19 UCSC genome to estimate gene expression values, which were then used to form a non-normalized count matrix. Similarly, RSEM with default parameters was run on sequencing reads of conditions involved in the derivation of astrocytic cells using the human hg19 UCSC genome to estimate gene expression values, which was then used to generate a non-normalized count matrix.

Further bulk RNA-seq data analysis was performed using DESeq2 package[58] and R v.3.2. Following DESeq2 protocols[58], significant genes from the differential expression analysis were identified using DESeq2's own two-sided statistical test and taking the false discovery rate (FDR) adjusted *P* value cut-off of 0.05 for all analyses in this study. As previously described[58], DESeq2 relies on the negative binomial distribution and utilizes Benjamini–Hochberg adjustment. PCA was carried out using DESeq2 package and R. Database for Annotation, Visualization and Integrated Discovery v.6.7 and v.6.8 and the Molecular Signatures Database (MSigDB) were used to reveal enriched biological processes for differentially expressed genes (either upregulated or downregulated in one condition). GSEA was performed using GSEA software[59] v.2.2.3 using default parameters to find enriched biological processes in GO and enriched Kyoto Encyclopedia of Genes and Genomes (KEGG) pathways in compared conditions. The *k*-means function in R was used to cluster groups of genes. Groups were generated by first performing differential expression analysis between a reference condition and other conditions and then filtering the resulting differentially expressed genes by setting $\log_2$(fold change) and *P* cut-off values.

To compare the transcriptomes of 3D cultures of iN cells to the human brain developmental transcriptome, gene level expression values were obtained from the BrainSpan database (http://www.brainspan.org/static/download.html). To our knowledge, raw data for the BrainSpan transcriptome profiling dataset in the form of fastq or BAM files are not available for download. Therefore, in an effort to minimize technical differences between the experimental and reference datasets, RNA-seq data of 3D cultures of iN cells were reprocessed to more closely match that of BrainSpan following the alignment and gene quantification protocol described. Briefly, filtered fastq files of RNA-seq samples were realigned with Tophat v.2.0.14 using Bowtie v.0.12.9 and samtools v.0.1.9. To further match the BrainSpan dataset, the data were processed using Gencode v.10. RSEQtools, which was utilized by the BrainSpan group, to obtain gene level expression values. This process included converting the reprocessed BAM files into MRF files, and using the mrfQuantifier function to obtain the final gene expression matrix. The BrainSpan region expression matrix between developmental stages of 8 pcw and 1 year old was filtered to maximize the proportion of genes with high expression (RPKM > 5) and variance (> 1). Pearson correlations based on these 11,972 genes were obtained for each 3D culture condition of iN cells and developmental brain region–time point pair. All plots represent the mean correlation (± s.e.m.) of three replicates of 3D culture conditions of iN cells with a specific developmental brain region and time point.

For profiling expression levels of disease-associated genes in iN cells cultured in 3D conditions, ASD-associated genes were obtained from https://gene.sfari.org/autdb/GSGeneList.do?c=S, ALS-associated genes were obtained from the ALS Online Database[60] (http://alsod.iop.kcl.ac.uk/misc/dataDownload.aspx#C1) and the ALS Gene Database[61] (http://www.alsgene.org/top_results), Alzheimer disease-associated genes were obtained from a published study[62], and Parkinson disease-associated genes were obtained from the PD Gene Database[63] (http://www.pdgene.org/top_results). To determine which genes are driving the increased correlation in expression with BrainSpan data in iN cells co-cultured in the CH with 4X crosslinker compared with iN cells co-cultured in Matrigel, for each gene, we calculated both the squared log fold-change between iN cells co-cultured in Matrigel and BrainSpan data and the squared log fold-change between iN cells co-cultured in the CH with 4X crosslinker and BrainSpan data (using RPKM normalized data), and took the difference between the two values to obtain our final score.

scRNA-seq. 3D co-cultures of iN cells with mouse astrocytes and with human astrocytic cells were generated in 200 µl of CHs made using a 12.5 mM $CaCl_2$ solution. A 1:1 mixture of iN cells and mouse astrocytes was encapsulated (at a final cell concentration of 30×10^6 cells ml^{-1}) in corresponding CHs and cultured as described above. Astrocytic cells derived using the morphogen + FBS protocol were cultured until day 83 in passage 5, and were detached in passage 6 from culture plates with Accutase and pooled. A 1:1 mixture of iN cells and astrocytic cells was encapsulated (at a final cell concentration of 30×10^6 cells ml^{-1}) in corresponding CHs and cultured as described above, with the following change: the culture medium did not contain doxycycline. At week 5 of culture, cell disassociation from 3D tissues was performed utilizing a previously described protocol[16] with the following modifications. Briefly, each 3D tissue was cut into small pieces with a blade and immersed in 1 ml of 20:1 mix of papain solution (PAP2, Worthington) and DNase solution (D2, Worthington) in a 15 ml tube, which was then incubated at 37 °C for 20 min and shaken by hand every 5 min. After 20 min, pieces of 3D tissues in this solution were pipetted for further dissociation and then incubated at 37 °C for 10 min. A volume (1 ml) of Earle's balanced salt solution (EBSS, Worthington) was mixed with the solution of dissociated tissue. The cloudy cell suspension from this mix was transferred to a new 15 ml tube and mixed with 1.9 ml of inhibitor solution (OI.BSA, Worthington). This final solution was then centrifuged at 300 *g* for 5 min. Cell pellets from three biological replicates of each 3D co-culture condition (iN cells with mouse astrocytes and iN cells with human astrocytic cells) were pooled by resuspending the cell pellets in ice-cold DPBS with 0.2% BSA (Sigma), which was then passed through a 30 µm filter (Sysmex). Cell suspensions for each condition, 3D co-cultures of iN cells with mouse astrocytes and 3D co-cultures of iN cells with human astrocytic cells, were loaded onto a 10× Chromium Instrument (10× Genomics) through two independent channels to generate single-cell gel bead in emulsion. scRNA-seq libraries were constructed using 10× Chromium 3′ Solution (10× Genomics) following the manufacturer's protocol and sequenced on a NextSeq 500 instrument (Illumina) with 26 bases for read1 and 57 bases for read2.

Single-cell data analysis. Cellranger[54] was used to map fastq files to the joint hg19 and mm10 transcriptome, with the option --force-cells = 10,000. The cell by gene (hg19 genes only, mm10 genes were explored separately for quality control purposes) count matrix was loaded into R using Seurat v1.3[64]. The data were normalized to be log counts per million, and we removed all cells expressing fewer than 1,000 human genes or more than 300 mouse genes. MeanVarPlot was used to find variable genes (with x.low.cut-off = 1). The number of genes and percentage mitochondrial RNA were regressed out with the RegressOut function, and PCA was performed using PCAFast. Rtsne was applied to the PCA matrix using the top 13 principal components. Clustering was performed as previously described[65], using the top 13 principal components and a 100 shared nearest neighbour graph. Cell type clusters were identified using known marker genes. Note that the clusters identified as neurons express many IPC markers at high levels, but comparison with published datasets[38,39] (see below) suggests that these clusters are more similar to neurons than IPCs (see Results).

We loaded numerous published single-cell datasets of human fetal cortex[38,39] and a single-nucleus dataset of adult post-mortem human brain tissue[40], and a single-cell dataset of 6-month-old human brain organoids[16] into R with Seurat. All data were normalized to be log counts per million, and we removed all cells with fewer than 500 genes. MeanVarPlot was used to find variable genes (with x.low.cut-off = 1). For each dataset, we used the clustering available from their respective papers, and identified cell types based on marker genes. In addition, we extracted the forebrain cluster from the 6-month-old human brain organoid[16] dataset, and subclustered it using the same pipeline as used for our single-cell dataset, except we did not regress out percentage mitochondria, and used 12 principal components and 50 shared nearest neighbors for clustering.

Correlation heatmaps comparing clusters in our single-cell dataset to clusters in published single-cell[16,38,39] and single-nucleus[40] datasets were generated as follows: for each dataset, the Seurat function AverageCluster was used to generate the average expression profiles of clusters in that dataset. Variable genes from the published single-cell[16,38,39] or single-nucleus[40] dataset were identified by MeanVarPlot and then used to calculate the correlation between these average transcript profiles. For comparison between bulk RNA-seq of conditions involved in our astrocyte differentiation protocol and single-cell and single-nucleus datasets of the human brain, a similar procedure as described above was used to calculate the average expression of each cell type in the single-cell or single-nucleus data. These average profiles were then compared with the expression profiles from the bulk data (measured in log TPM) using Pearson correlation.

Reporting Summary. Further information on experimental design is available in the Nature Research Reporting Summary linked to this article.

Code availability. Codes are available in Github at https://github.com/3D-Neural-NBME.

Data availability. All data supporting the findings of this study are available within the paper and its Supplementary Information. RNA-seq data generated in this study are available through the Gene Expression Omnibus under accession code GSE111831. Human brain transcriptome data are available through the BrainSpan database (http://www.brainspan.org). Mouse reads filtered non-normalized count matrix and TPM matrix used for bulk RNA-seq analysis are available in Github at https://github.com/3D-Neural-NBME/Bulk-RNA-seq-analysis. The gene-expression matrix used for BrainSpan analysis is available in Github at https://github.com/3D-Neural-NBME/BrainSpan-analysis.

Received: 30 May 2017; Accepted: 12 March 2018;
Published online: 9 April 2018

References

1. Bulik-Sullivan, B. et al. An atlas of genetic correlations across human diseases and traits. *Nat. Genet.* **47**, 1236–1241 (2015).
2. Quadrato, G., Brown, J. & Arlotta, P. The promises and challenges of human brain organoids as models of neuropsychiatric disease. *Nat. Med.* **22**, 1220–1228 (2016).
3. Lambert, J. C. et al. Meta-analysis of 74,046 individuals identifies 11 new susceptibility loci for Alzheimer's disease. *Nat. Genet.* **45**, 1452–1458 (2013).
4. McCarro, S. A., Feng, G. P. & Hyman, S. E. Genome-scale neurogenetics: methodology and meaning. *Nat. Neurosci.* **17**, 756–763 (2014).
5. Gandhi, S. & Wood, N. W. Genome-wide association studies: the key to unlocking neurodegeneration?. *Nat. Neurosci.* **13**, 789–794 (2010).
6. Choi, S. H. et al. A three-dimensional human neural cell culture model of Alzheimer's disease. *Nature* **515**, 274–278 (2014).
7. Tang-Schomer, M. D. et al. Bioengineered functional brain-like cortical tissue. *Proc. Natl Acad. Sci. USA* **111**, 13811–13816 (2014).
8. Schwartz, M. P. et al. Human pluripotent stem cell-derived neural constructs for predicting neural toxicity. *Proc. Natl Acad. Sci. USA* **112**, 12516–12521 (2015).
9. Kim, S. H. et al. Anisotropically organized three-dimensional culture platform for reconstruction of a hippocampal neural network. *Nat. Commun.* **8**, 14346 (2017).
10. Grealish, S. et al. Human ESC-derived dopamine neurons show similar preclinical efficacy and potency to fetal neurons when grafted in a rat model of Parkinson's disease. *Cell Stem Cell* **15**, 653–665 (2014).
11. Dimos, J. T. et al. Induced pluripotent stem cells generated from patients with ALS can be differentiated into motor neurons. *Science* **321**, 1218–1221 (2008).
12. Pasca, A. M. et al. Functional cortical neurons and astrocytes from human pluripotent stem cells in 3D culture. *Nat. Methods* **12**, 671–678 (2015).
13. Lancaster, M. A. et al. Cerebral organoids model human brain development and microcephaly. *Nature* **501**, 373–379 (2013).
14. Qian, X. Y. et al. Brain-region-specific organoids using mini-bioreactors for modeling ZIKV exposure. *Cell* **165**, 1238–1254 (2016).
15. Kraehenbuehl, T. P., Langer, R. & Ferreira, L. S. Three-dimensional biomaterials for the study of human pluripotent stem cells. *Nat. Methods* **8**, 731–736 (2011).
16. Quadrato, G. et al. Cell diversity and network dynamics in photosensitive human brain organoids. *Nature* **545**, 48–53 (2017).
17. Camp, J. G. et al. Human cerebral organoids recapitulate gene expression programs of fetal neocortex development. *Proc. Natl Acad. Sci. USA* **112**, 15672–15677 (2015).
18. Busskamp, V. et al. Rapid neurogenesis through transcriptional activation in human stem cells. *Mol. Syst. Biol.* https://doi.org/10.15252/msb.20145508 (2014).
19. Zhang, Y. S. et al. Rapid single-step induction of functional neurons from human pluripotent stem cells. *Neuron* **78**, 785–798 (2013).
20. Pang, Z. P. P. et al. Induction of human neuronal cells by defined transcription factors. *Nature* **476**, 220–223 (2011).
21. Chanda, S. et al. Generation of induced neuronal cells by the single reprogramming factor ASCL1. *Stem Cell Reports* **3**, 282–296 (2014).
22. Lam, R. S., Töpfer, F. M., Wood, P. G., Busskamp, V. & Bamberg, E. Functional maturation of human stem cell-derived neurons in long-term cultures. *PLoS ONE* **12**, e0169506 (2017).
23. Yi, F. et al. Autism-associated SHANK3 haploinsufficiency causes I_h channelopathy in human neurons. *Science* **352**, aaf2669 (2016).
24. Huang, Y.-W. A., Zhou, B., Wernig, M. & Südhof, T. C. ApoE2, ApoE3, and ApoE4 differentially stimulate APP transcription and Aβ secretion. *Cell* **168**, 427–441.e421 (2017).
25. Carlson, A. L. et al. Generation and transplantation of reprogrammed human neurons in the brain using 3D microtopographic scaffolds. *Nat. Commun.* **7**, 10862 (2016).
26. Lau, L. W., Cua, R., Keough, M. B., Haylock-Jacobs, S. & Yong, V. W. Pathophysiology of the brain extracellular matrix: a new target for remyelination. *Nat. Rev. Neurosci.* **14**, 722–729 (2013).
27. Tang, X. et al. Astroglial cells regulate the developmental timeline of human neurons differentiated from induced pluripotent stem cells. *Stem Cell Res.* **11**, 743–757 (2013).
28. Margolis, R. U., Margolis, R. K., Chang, L. B. & Preti, C. Glycosaminoglycans of brain during development. *Biochemistry* **14**, 85–88 (1975).
29. Bozza, A. et al. Neural differentiation of pluripotent cells in 3D alginate-based cultures. *Biomaterials* **35**, 4636–4645 (2014).
30. Brannvall, K. et al. Enhanced neuronal differentiation in a three-dimensional collagen–hyaluronan matrix. *J. Neurosci. Res.* **85**, 2138–2146 (2007).
31. Seidlits, S. K. et al. The effects of hyaluronic acid hydrogels with tunable mechanical properties on neural progenitor cell differentiation. *Biomaterials* **31**, 3930–3940 (2010).
32. Khetan, S. et al. Degradation-mediated cellular traction directs stem cell fate in covalently crosslinked three-dimensional hydrogels. *Nat. Mater.* **12**, 458–465 (2013).
33. Chaudhuri, O. et al. Extracellular matrix stiffness and composition jointly regulate the induction of malignant phenotypes in mammary epithelium. *Nat. Mater.* **13**, 970–978 (2014).
34. Chaudhuri, O. et al. Hydrogels with tunable stress relaxation regulate stem cell fate and activity. *Nat. Mater.* **15**, 326–334 (2016).
35. Huebsch, N. et al. Harnessing traction-mediated manipulation of the cell/matrix interface to control stem-cell fate. *Nat. Mater.* **9**, 518–526 (2010).
36. Shaltouki, A., Peng, J., Liu, Q. Y., Rao, M. S. & Zeng, X. M. Efficient generation of astrocytes from human pluripotent stem cells in defined conditions. *Stem Cells* **31**, 941–952 (2013).
37. Chojnacki, A. & Weiss, S. Production of neurons, astrocytes and oligodendrocytes from mammalian CNS stem cells. *Nat. Protoc.* **3**, 935–940 (2008).
38. Pollen, A. A. et al. Molecular identity of human outer radial glia during cortical development. *Cell* **163**, 55–67 (2015).
39. Nowakowski, T. J. et al. Spatiotemporal gene expression trajectories reveal developmental hierarchies of the human cortex. *Science* **358**, 1318–1323 (2017).
40. Habib, N. et al. Massively parallel single-nucleus RNA-seq with DroNc-seq. *Nat. Methods* **14**, 955–958 (2017).
41. Zetsche, B. et al. Multiplex gene editing by CRISPR-Cpf1 using a single crRNA array. *Nat. Biotechnol.* **35**, 31–34 (2017).
42. Zetsche, B. et al. Cpf1 Is a single RNA-guided endonuclease of a class 2 CRISPR–Cas system. *Cell* **163**, 759–771 (2015).
43. Renton, A. E., Chio, A. & Traynor, B. J. State of play in amyotrophic lateral sclerosis genetics. *Nat. Neurosci.* **17**, 17–23 (2014).
44. Katz, J. S., Katzberg, H. D., Woolley, S. C., Marklund, S. L. & Andersen, P. M. Combined fulminant frontotemporal dementia and amyotrophic lateral sclerosis associated with an I113T *SOD1* mutation. *Amyotroph. Lateral Scler.* **13**, 567–569 (2012).
45. Mackenzie, I. R. A., Rademakers, R. & Neumann, M. TDP-43 and FUS in amyotrophic lateral sclerosis and frontotemporal dementia. *Lancet Neurol.* **9**, 995–1007 (2010).
46. Freischmidt, A. et al. Haploinsufficiency of TBK1 causes familial ALS and fronto-temporal dementia. *Nat. Neurosci.* **18**, 631–636 (2015).
47. Burdick, J. A. & Prestwich, G. D. Hyaluronic acid hydrogels for biomedical applications. *Adv. Mater.* **23**, H41–H56 (2011).
48. Brigham, M. D. et al. Mechanically robust and bioadhesive collagen and photocrosslinkable hyaluronic acid semi-interpenetrating networks. *Tissue Eng. Part A* **15**, 1645–1653 (2009).
49. Back, S. A. et al. Hyaluronan accumulates in demyelinated lesions and inhibits oligodendrocyte progenitor maturation. *Nat. Med.* **11**, 966–972 (2005).
50. Zaman, M. H. et al. Migration of tumor cells in 3D matrices is governed by matrix stiffness along with cell-matrix adhesion and proteolysis. *Proc. Natl Acad. Sci. USA* **103**, 10889–10894 (2006).
51. Catanzano, O. et al. Alginate–hyaluronan composite hydrogels accelerate wound healing process. *Carbohydr. Polym.* **131**, 407–414 (2015).
52. Gao, L. Y. et al. Engineered Cpf1 variants with altered PAM specificities. *Nat. Biotechnol.* **35**, 789–792 (2017).
53. Patel, A. P. et al. Single-cell RNA-seq highlights intratumoral heterogeneity in primary glioblastoma. *Science* **344**, 1396–1401 (2014).
54. Zheng, G. X. Y. et al. Massively parallel digital transcriptional profiling of single cells. *Nat. Commun.* **8**, 14049 (2017).
55. Picelli, S. et al. Full-length RNA-seq from single cells using Smart-seq2. *Nat. Protoc.* **9**, 171–181 (2014).
56. Li, B. & Dewey, C. N. RSEM: accurate transcript quantification from RNA-Seq data with or without a reference genome. *BMC Bioinformatics* **12**, 323 (2011).
57. Dobin, A. et al. STAR: ultrafast universal RNA-seq aligner. *Bioinformatics* **29**, 15–21 (2013).
58. Love, M. I., Huber, W. & Anders, S. Moderated estimation of fold change and dispersion for RNA-seq data with DESeq2. *Genome Biol.* **15**, 550 (2014).
59. Subramanian, A., Kuehn, H., Gould, J., Tamayo, P. & Mesirov, J. P. GSEA-P: a desktop application for gene set enrichment analysis. *Bioinformatics* **23**, 3251–3253 (2007).
60. Abel, O., Powell, J. F., Andersen, P. M. & Al-Chalabi, A. ALSoD: a user-friendly online bioinformatics tool for amyotrophic lateral sclerosis genetics. *Hum. Mutat.* **33**, 1345–1351 (2012).
61. Lill, C. M., Abel, O., Bertram, L. & Al-Chalabi, A. Keeping up with genetic discoveries in amyotrophic lateral sclerosis: the ALSoD and ALSGene databases. *Amyotroph. Lateral Scler.* **12**, 238–249 (2011).
62. Van Cauwenberghe, C., Van Broeckhoven, C. & Sleegers, K. The genetic landscape of Alzheimer disease: clinical implications and perspectives. *Genet. Med.* **18**, 421–430 (2016).
63. Nalls, M. A. et al. Large-scale meta-analysis of genome-wide association data identifies six new risk loci for Parkinson's disease. *Nat. Genet.* **46**, 989–993 (2014).

64. Satija, R., Farrell, J. A., Gennert, D., Schier, A. F. & Regev, A. Spatial reconstruction of single-cell gene expression data. *Nat. Biotechnol.* **33**, 495–502 (2015).
65. Shekhar, K. et al. Comprehensive classification of retinal bipolar neurons by single-cell transcriptomics. *Cell* **166**, 1308–1323.e30 (2016).

Acknowledgements

We thank R. Macrae for critical reading of the manuscript and R. Belliveau for technical support. We thank R. Langer for input during the preparation of the manuscript and the entire Zhang Laboratory for assistance in the laboratory and helpful discussions. F.Z. is a New York Stem Cell Foundation–Robertson Investigator. F.Z. is supported by the following grants and institutes: NIH grant nos. 1R01-HG009761, 1R01-MH110049 and 1DP1-HL141201; the Howard Hughes Medical Institute; the New York Stem Cell, Simons, Paul G. Allen Family, and Vallee Foundations; and J. and P. Poitras, R. Metcalfe, and D. Cheng. J.Z.L and J.Q.P. are supported by The Stanley Center for Psychiatric Research at the Broad Institute. We thank the Klarman Cell Observatory for supporting experiments using the 10× Chromium Instrument. Reagents are available through Addgene and codes can be accessed via GitHub.

Author contributions

H.T. and F.Z. conceived the study. H.T. designed the experiments, developed 3D and 2D cultures and 3D co-cultures of iN cells and the method to derive astrocytic cells, analysed the RNA-seq data, performed qPCR, immunostaining and imaging. S.S. filtered mouse reads from bulk RNA-seq data of iN cells co-cultured with mouse astrocytes. B.C. and H.T. performed and interpreted the comparisons between the transcriptomes of 3D cultures and co-cultures of iN cells and the human brain developmental transcriptome. X.A., C.C.H. and J.Z.L. constructed bulk RNA-seq libraries and performed sequencing. D.D. constructed scRNA-seq libraries and C.C.H. performed sequencing. J.Z.L aligned the scRNA-seq data to reference genomes. S.S. and H.T. analysed and interpreted the scRNA-seq data. L.G., S.R.C. and M.H. cloned the DNA constructs. L.G. and H.T. tested single guide RNAs in HEK cells. S.R.C. produced the AAVs. H.T. developed 3D tissues of iN cells and astrocytic cells, performed AAV infection of iN cells in 3D tissues and isolated targeted iN cells by FACS. L.G. performed next-generation sequencing and indel analyses. A.G. and J.Q.P. performed electrophysiology experiments. V.Y. and H.T. performed the mechanical characterization of the hydrogels. N.E.S. and X.S. developed hESCs with inducible expression of *NGN1* and *NGN2*. C.L. isolated and expanded mouse glia. H.T. wrote the paper with input from all authors.

Competing interests

H.T. and F.Z. are co-inventors in a patent application relating to work in this manuscript. The remaining authors declare no competing interests.

Additional information

Supplementary information is available for this paper at https://doi.org/10.1038/s41551-018-0219-9.

Reprints and permissions information is available at www.nature.com/reprints.

Correspondence and requests for materials should be addressed to H.T.

Publisher's note: Springer Nature remains neutral with regard to jurisdictional claims in published maps and institutional affiliations.